

Formation of the Galactic Stellar Halo. I. Structure and Kinematics

Kenji Bekki

School of Physics, University of New South Wales, Sydney 2052, Australia

and

Masashi Chiba

National Astronomical Observatory, Mitaka, Tokyo, 181-8588, Japan

ABSTRACT

We perform numerical simulations for the formation of the Galactic stellar halo, based on the currently favored cold dark matter (CDM) theory of galaxy formation. Our numerical models, taking into account both dynamical and chemical evolution processes in a consistent manner, are aimed at explaining observed structure and kinematics of the stellar halo in the context of hierarchical galaxy formation. The main results of the present simulations are summarized as follows.

(1) Basic physical processes involved in the formation of the stellar halo, composed of metal-deficient stars with $[\text{Fe}/\text{H}] \leq -1.0$, are described by both dissipative and dissipationless merging of subgalactic clumps and their resultant tidal disruption in the course of gravitational contraction of the Galaxy at high redshift ($z > 1$).

(2) The simulated halo has the density profile similar to the observed power-law form of $\rho(r) \sim r^{-3.5}$, and has also the similar metallicity distribution to the observations. The halo virtually shows no radial gradient for stellar ages and only small gradient for metallicities.

(3) The dual nature of the halo, i.e., its inner flattened and outer spherical density distribution, is reproduced, at least qualitatively, by the present model. The outer spherical halo is formed via essentially dissipationless merging of small subgalactic clumps, whereas the inner flattened one is formed via three different mechanisms, i.e., dissipative merging between larger, more massive clumps, adiabatic contraction due to the growing Galactic disk, and gaseous accretion onto the equatorial plane.

(4) For the simulated metal-poor stars with $[\text{Fe}/\text{H}] \leq -1.0$, there is no strong correlation between metal abundances and orbital eccentricities, in

good agreement with the recent observations. Moreover, the observed fraction of the low-eccentricity stars is reproduced correctly for $[\text{Fe}/\text{H}] \leq -1.6$ and approximately for the intermediate abundance range of $-1.6 < [\text{Fe}/\text{H}] \leq -1.0$.

(5) The mean rotational velocity of the simulated halo, $\langle V_\phi \rangle$, is somewhat positive (prograde) at $[\text{Fe}/\text{H}] < -2.2$ and increases linearly with $[\text{Fe}/\text{H}]$ at $[\text{Fe}/\text{H}] > -2.2$. The stars at smaller distance from the disk plane appear to show systematically larger $\langle V_\phi \rangle$.

Based on these results, we discuss how early processes of dissipationless and dissipative merging of subgalactic clumps can reproduce plausibly and consistently the recent observational results on the Galactic stellar halo. We also present a possible scenario for the formation of the entire Galaxy structure, including bulge and disk components, in conjunction with the halo formation.

Subject headings: Galaxy: abundance – Galaxy: evolution – Galaxy: halo

1. Introduction

Formation and evolution of the metal-deficient halo remain elusive, although it constitutes a fundamental component in the Galaxy. Its detailed structure and kinematics are clues to the understanding of how the Galaxy has developed its dynamical structures (e.g., Freeman 1987; Majewski 1993; van den Bergh 1996). In particular, observed correlation between chemical and dynamical properties of halo stars or lack thereof provides valuable information on the early dynamical history of the Galaxy, because the metallicity can be regarded as a sort of “clock” of the Galaxy (Gilmore, King, & van der Kruit 1990). Also, studies of kinematic substructures in the stellar halo allow us to elucidate the detailed history of merging between the Galaxy and any subgalactic fragments, such as dwarf galaxies, because the time scale for mixing of halo stars due to momentum and energy exchange exceeds the age of the Galaxy (e.g., Lynden-Bell & Lynden-Bell 1995; Johnston, Spiegel, & Hernquist 1995; Helmi et al. 1999; Morrison et al. 2000).

Based on penetrative analysis of such important populations of the Galactic “fossil record”, two canonical scenarios of the Galactic halo formation were proposed, that have long been influential for later observational and theoretical studies of disk and elliptical galaxies. One is the monolithic collapse picture proposed by Eggen, Lynden-Bell, & Sandage (1962, hereafter ELS), in which the halo is formed from an overdense homogeneous sphere very rapidly within an order of free-fall time ($\sim 10^8$ yr). The other is the accretion/merging scenario by Searle & Zinn (1978, hereafter SZ), in which the halo is formed slowly ($\sim 10^9$

yr) by chaotic merging/accretion of several subgalactic fragments. Although a considerable number of works have discussed advantages and disadvantages of these scenarios in explaining accumulated observational results (e.g., Yoshii & Saio 1979; Norris, Bessell, & Pickles 1985; Norris & Ryan 1991; Beers & Sommer-Larsen 1995), it is yet unsettled which picture, ELS or SZ, can describe more correctly and plausibly the early dynamical evolution the Galaxy (e.g., van den Bergh 1996).

In order to settle the above issue, we require a large and reliable set of data for metal-poor halo stars chosen with criteria that do not unduly influence the subsequent analysis (e.g., Norris 1986; Chiba & Yoshii 1998, hereafter CY). In particular, the large data set of halo stars with various metallicities chosen without any kinematical selection bias are required for reliable discussion on the issue. Such kinematic aspects of the Galactic metal-poor stars have been greatly improved by the recently completed *Hipparcos* Catalogue (ESA 1997) and various ground-based catalogs (e.g., Platais et al. 1998; Urban et al. 1998) which provide unprecedentedly accurate proper motion data for a wealth of metal-poor stars (Beers et al. 2000). Recent works using non-kinematically selected samples of stars with available proper motions revisited the issue and demonstrated that either of the two scenarios alone has several difficulties in explaining the up-to-date observational results (Chiba & Beers 2000, hereafter CB).

For example, the ELS scenario is inconsistent with the observed no correlation between metallicities and orbital eccentricities of halo stars (CY; CB), and also the lack of the halo abundance gradient (CY). Equally, the SZ scenario unlikely explains the observed vertical gradient of rotational velocity as well as the inner flattened density distribution of halo stars (CB). This failure of the two models suggests several researchers to consider alternative models such as a hybrid scenario of the halo formation in which dissipationless merging of subgalactic clumps forms the outer Galactic halo, whereas ordered dissipative collapse forms the inner one (e.g., Norris 1994; Freeman 1996; Carney et al. 1996). However, while such a hybrid scenario may reproduce most of observational results, it is indispensable for the scenario to explain whether both of these dissipationless and dissipative processes actually take place in the early dynamical evolution of the Galaxy.

Besides these two canonical scenarios, the formation of the stellar halo has not been discussed so extensively in the framework of the currently favored theory based on hierarchical assembly of cold dark matter (CDM) halos (e.g., White & Rees 1978; Peacock 1999). In the hierarchical clustering scenario, as the gravitational collapse of a protogalaxy proceeds, numerous subgalactic clumps are developed from initial small-scale density perturbations predicted by the CDM model. These clumps merge with one another dissipatively or dissipationlessly to grow in a hierarchical manner and finally form the

Galaxy. Recent numerical simulations of the Galaxy formation based on the hierarchical clustering scenario demonstrated that metal-poor stars which finally build the stellar halo component have already been formed at very high redshift ($z > 2$) within each of merging subgalactic clumps (Steinmetz & Müller 1995; Bekki & Chiba 2000a). These studies also suggested that the dispersal of metal-poor stars caused by tidal disruption of clumps is responsible for the formation of the stellar halo.

Previous simulations conducted to date have provided a rough sketch of the Galaxy formation and demonstrated the importance of initial small density perturbations in the formation processes of galactic bulges and disks (e.g., Katz 1992). Furthermore semi-analytic models of galaxy formation and evolution based on CDM models have provided important predictions on bulge and disk formation (e.g., Kauffmann et al. 1993; Baugh et al. 1998; Somerville & Primack 1999). However, it was yet unexplored whether or not the CDM model can provide a definite and realistic picture for the formation of the Galactic stellar halo, including all of its structural, kinematical, and chemical properties.

Thus, the purpose of this paper is (1) to investigate thoroughly whether the CDM model can reproduce successfully the recent observational results on the Galactic halo and (2) to provide a general picture of the Galaxy formation including stellar halo, bulge, and disk components. We perform numerical simulations of the Galaxy based on the standard CDM model and investigate structure and kinematics of the developed metal-poor stellar halo. In particular, we compare our numerical simulations with recent observational results by CY and CB and elucidate the detailed mechanism of the halo formation.

We note that Côte et al. (2000) recently investigated the origin of metallicity distribution of the Galactic stellar halo in the context of hierarchical merging of dwarf-like galaxies. However, the detailed kinematical properties of the halo were unexplored. Also, most of the CDM-based numerical models on disk galaxy formation have focused on only the fundamental properties of a disk, such as an exponential density profile (Katz 1992) and Tully-Fisher relation (Steinmetz & Navarro 1999). The spatial structure of the stellar halo has been examined by Steinmetz & Müller (1995), but, again, the detailed kinematics of the halo stars in the simulated model remained unknown. Thus we believe that our approach to modeling all of the structural, kinematical, and chemical properties of the halo can provide valuable clues to the formation of the Galaxy.

The layout of this paper is as follows. In §2, we summarize numerical models used in the present study and describe the methods for analyzing structure and kinematics of the simulated stellar halo. In §3, we present numerical results on the time evolution of morphology, metallicity distribution, and dynamical properties of the forming halo. In §4, we discuss success and failure of the present model in reproducing the observed dynamical

properties of the Galactic halo and provide a possible scenario of the Galaxy formation. The conclusions of the preset study are given in §5.

2. Model

2.1. Numerical methods

The numerical method and technique for solving galactic chemodynamical evolution and models for describing star formation and dissipative gas dynamics are presented in Bekki & Shioya (1998), so here we briefly describe the initial conditions of protogalactic clouds, star formation law, and chemical evolution model. The way to set up initial conditions for numerical simulations of forming disk galaxy within a hierarchical clustering scenario is essentially the same as that adopted by Katz & Gunn (1991) and Steinmetz & Müller (1995). We here use the COSMICS (Cosmological Initial Conditions and Microwave Anisotropy Codes), which is a package of fortran programs for generating Gaussian random initial conditions for nonlinear structure formation simulations (Bertschinger 1995; Ma & Bertschinger 1995). We consider an isolated homogeneous, rigidly rotating sphere, on which small-scale fluctuations according to a CDM power spectrum are superimposed. The mass ratio of dark matter to baryons is 9.0 and both components have the same initial distribution. The initial total mass, radius, and spin parameter (λ) of the sphere in the present model are $6.0 \times 10^{11} M_{\odot}$, 45 kpc, and 0.08, respectively. For cosmological parameters of $\Omega = 1.0$, $q_0 = 0.5$, and $H_0 = 50 \text{ km s}^{-1} \text{ Mpc}^{-1}$ adopted in the present study, the initial overdensity δ_i of the sphere in the fiducial model is estimated to be 0.29 corresponding to a 2.5σ overdensity of a biased CDM spectrum on a mass-scale of $6.0 \times 10^{11} M_{\odot}$ with a biasing parameter $b = 2$. We start the simulation at the redshift $z = 25$ and follow it till $z = 0$ corresponding to the age of the universe equal to 13 Gyr. Initial conditions similar to those adopted in the present study are demonstrated to be plausible and realistic for the formation of the Galaxy (e.g., Steinmetz & Müller 1995).

Star formation is modeled by converting the collisional gas particles into collisionless new stellar particles according to the Schmidt law (Schmidt 1959) with the exponent of 2 and the coefficients in the law are taken from the work of Bekki (1998). The collisional and dissipative nature of the interstellar medium are modeled according to the sticky particle method (Schwarz 1981) with the cloud radius (r_{cl}) of 450 pc and we consider multiple collisions among clouds (see Bekki & Shioya 1998 for details). It should be emphasized here that this discrete cloud model can at best represent the *real* interstellar medium of galaxies in a schematic way. As is modeled by McKee & Ostriker (1977), the interstellar medium is composed mainly of ‘hot’, ‘warm’, and ‘cool’ gas, each of which mutually

interacts hydrodynamically in a rather complicated way. Actually, such a considerably complicated nature of the interstellar medium in forming disk galaxies would not be so simply represented by the “sticky particle” model in which gaseous dissipation is modeled by ad hoc cloud-cloud collision: Any existing numerical method probably could not model the *real* interstellar medium in an admittedly proper way. In the present study, as a compromise, we only try to address some important aspects of hydrodynamical interaction between interstellar clouds in forming disk galaxies. More elaborated numerical modeling of the interstellar medium would be necessary for our further understanding of dynamical evolution in forming disk galaxies.

We note that the phenomenological sticky particle model adopted here is in great contrast with SPH models used in previous numerical works of galaxy formation (e.g., Katz 1992; Steinmetz & Müller 1995). Although the sticky particle model has succeeded in addressing some important aspects of hydrodynamical interaction in interstellar medium, such as dynamical interaction between giant molecular clouds (e.g., Roberts & Hausman 1984; Combes & Gerin 1985), its weak point is considered to be an ad hoc estimate of an energy dissipation in cloud collisions (e.g., Shlosman & Noguchi 1993). On the other hand, the SPH method, which often introduces the virtual cut-off of cooling function around 10^4 K (e.g., Katz 1992) and thus can investigate only warm gas components ($T > 10^3 - 10^4$ K), cannot follow formation and evolution of cold molecular components that may well dominate the interstellar medium in very gas-rich young disk galaxies. Accordingly the SPH method holds difficulties in simulating interaction between *discrete* gas clouds in a self-consistent manner. Thus, we consider that both the SPH and sticky particle models are complimentary with each other in representing the real interstellar medium of forming galaxies.

Chemical enrichment through star formation during merging of subgalactic clumps is assumed to proceed both locally and instantaneously in the present study. The model for analyzing metal enrichment of each gas and stellar particle is as follows. First, as soon as a gas particle is converted into a new stellar one by star formation, we search neighboring gas particles locating within 0.01 in our units (corresponding to 450pc) from the position of the new stellar particle and then count the number of neighboring gas particles, N_{gas} . Next, we assign the metallicity of the original gas particle to the new stellar particle and increase the metal of each neighboring gas particle according to the following equation about the chemical enrichment:

$$\Delta M_Z = \{Z_i R_{\text{met}} m_s + (1.0 - R_{\text{met}})(1.0 - Z_i) m_s y_{\text{met}}\} / N_{\text{gas}} \quad (1)$$

where ΔM_Z represents the increase of metal for each gas particle. Z_i , R_{met} , m_s , and y_{met} represent the metallicity of the new stellar particle (or that of the original gas particle),

the fraction of gas returned to the interstellar medium, the mass of the new star, and the chemical yield, respectively. The values of R_{met} and y_{met} are set to be 0.3 and 0.02, respectively.

The total particle number used for modeling the initial sphere is 14147 both for dark matter and for baryons (gas and new stars), which means that the mass of each particle is $3.8 \times 10^7 M_{\odot}$ for dark matter and $4.2 \times 10^6 M_{\odot}$ for baryons. All the calculations related to the above chemodynamical evolution have been carried out on the GRAPE board (Sugimoto et al. 1990) at Astronomical Institute of Tohoku University. The parameter of gravitational softening is set to be fixed at 0.053 in our units (2.4 kpc). The time integration of the equation of motion is performed by using the 2nd-order leap-frog method.

As Figure 1 reveals, showing the evolution of dark matter particles, our simulation does not allow the persistence of small-scale structures at $z = 0$, as in Katz (1992) and Steinmetz & Müller (1995) using similar particle numbers, but in sharp contrast to recent high-resolution N-body studies (Klypin et al. 1999; Moore et al. 1999). These authors resolved the detailed clustering process of dark halo clumps with masses down to the order of $\sim 10^8 M_{\odot}$. The reasons for this difference are that the total particle number in the present study ($N \sim \text{a few} \times 10^4$) is considerably smaller than those adopted by such high-resolution simulations ($N \sim 10^6$ or mesh number of 128^3), and that the rather large length of gravitational softening (2.4 kpc) in our study erases small-scale structures with masses of $10^7 \sim 10^8 M_{\odot}$ even if they are developed. While it is yet unknown how such small-scale structures are modified by inclusion of gas dynamics and star formation, our primary concern here is to figure out the general formation process of the stellar halo in the framework of clustering theory, without going into the fine details of the halo structure. Perhaps, any additional phenomena associated with masses of $10^7 \sim 10^8 M_{\odot}$, such as excessive substructures of the halo and/or dynamical heating of the disk, may be precluded in a class of CDM theory (Kamionkowski & Liddle 1999; Spergel & Steinhardt 2000).

2.2. Main points of our analysis

Based on the above model, we mainly investigate structural and kinematical properties of the simulated metal-poor component: the mass fraction of the simulated metal-poor stars with $[\text{Fe}/\text{H}] \leq -1.6$, compared with the total baryonic mass of the system, is 0.014 at $z = 0$ and their mean age is about 10.5 Gyr. We focus on the nature of these old and metal-poor stars based on the present simulations, to investigate whether or not the CDM theory can reproduce reasonably well the observed fundamental characteristics of the Galactic halo. We investigate the following five points: (1) How does each of the Galactic components,

halo, bulge, and disk, form during merging between subgalactic clumps and what is the mutual relationship among the formation processes of these components?, (2) How is the inner flattened and outer spherical halo developed?, (3) Can the CDM model reproduce the observed dependence of $\langle V_\phi \rangle$ on $[\text{Fe}/\text{H}]$?, (4) What are the characteristics of the velocity ellipsoid of the simulated halo?, and (5) Are there any kinematic substructures in the simulated halo?

As a part of our analysis described in the next section, we calculate orbital eccentricities, e , of the stars with $[\text{Fe}/\text{H}] \leq -0.6$ at the epoch $z = 0$. Here e for each stellar particle is defined as:

$$e = \frac{r_{apo} - r_{peri}}{r_{apo} + r_{peri}} \quad (2)$$

where r_{apo} and r_{peri} are apo-galactic and peri-galactic distances from the center of the simulated Galaxy, respectively. For estimating e , we first select the stellar particles with $[\text{Fe}/\text{H}] \leq -0.6$ found at $z = 0$. Then we calculate the time evolution of their orbits under the gravitational potential of the simulated disk Galaxy achieved at $z = 0$ for ten dynamical time scale (~ 1.8 Gyr), and then estimate e . In order to avoid the contamination of metal-poor bulge stars in this estimation, we select only particles with their apo-galactic distances ranging from 8.5 to 17.5 kpc.

We use the symbol $[\text{Fe}/\text{H}]$ as the total metal abundance instead of the symbol Z , to avoid confusion with distance from the disk plane, although the current model does not consider the evolution of each element separately.

3. Result

3.1. Formation process of the entire Galaxy structure

We first describe the formation process of the entire Galaxy structure, consisting of dark matter halo, stellar halo, bulge, and disk components. Figure 1, 2, and 3 show dynamical evolution of dark matter, gas, and stars formed from gas, respectively, in the present model. The turn-around and collapse redshifts of the protogalactic sphere are 3.25 and 1.68, respectively. As the sphere expands, numerous small clumps composed of dark matter develop from non-linear gravitational growth of initial local density maxima at high redshift, $z \sim 10$. Owing to the strong gravitational attraction of dark matter, gas particles also assemble into each of the clumps. Then, gaseous dissipation due to collisions between gas particles proceeds, which results in the central concentration of gas even in this early dynamical stage ($5 < z < 10$). Consequently, first stars are formed in the central part of each clump.

Firstly born stars with old ages (> 10 Gyr) and low metallicities ($[\text{Fe}/\text{H}] < -3$) are confined within these small clumps until they are disrupted by later mutual merging. The clumps continue to merge with one another and grow up to become more massive clumps ($z = 2.56, 4.47$). Star formation proceeds efficiently in these growing clumps ($z = 1.75$), and consequently two most massive clumps are formed after multiple merging events of small clumps ($z = 1.75$). These two clumps dissipatively merge with each other and then leave a central bulge-like component ($z = 1.28$). Other surviving, less massive clumps continue to merge with one another and also with the two massive clumps even after the strong merging event of these massive clumps. Gas falling onto the surroundings of the bulge forms a disk-like component composed of gas and gradually forming stars ($0.75 < z < 0.94$). This young, disk-like component grows gradually owing to the continuous gas accretion from the halo region and finally becomes a well-developed disk with its size and mass similar to those of typical present-day disk galaxies like our own ($0 < z < 0.45$). This chemodynamical evolution of the Galaxy is basically in agreement with earlier numerical results by Katz (1992) and Steinmetz & Müller (1995).

Figure 4 shows the star formation history of the present model. While the Universe is still young, of the age of 0.3–0.4 Gyr ($z \sim 10$), some gas inside subgalactic clumps developed from small-scale density maxima is already consumed to form stars at a small rate of $\sim 2 M_{\odot} \text{ yr}^{-1}$. These very old and metal-poor stars may well be regarded as the first stars in the Galaxy¹. Star formation rate of the forming Galaxy exceeds $5 M_{\odot} \text{ yr}^{-1}$ at $1.5 < z < 2.0$ (corresponding to ~ 3 Gyr after the onset of the collapse) and takes the maximum value of $\sim 16 M_{\odot} \text{ yr}^{-1}$ when the two massive clumps merge with each other ($z \sim 1.5$). It is worthwhile here to remark that this starburst epoch of $z \sim 1.5$ matches the formation epoch of the bulge-like component in the simulated Galaxy. This starburst also drives rapid chemical evolution in the central part of the Galaxy and thereby greatly enriches gas and stars. As a consequence, this bulge-like component is made very metal rich.

After the star formation rate reaches the peak value, it gradually, at a nearly constant rate, declines to a few $M_{\odot} \text{ yr}^{-1}$, because minor merging which triggers sporadic increase of star formation does not frequently occur after $z = 1.28$. Stars formed from this gradual and long-term star formation build up the present-day disk component in our model. In this regard, Blitz et al. (1999) argued that the so-called High Velocity Clouds (HVCs) having large negative radial velocities may correspond to external primordial gas which continues to accrete toward the Galactic disk. If this process, which is not included in our simulation,

¹Many of these first stars are too metal-poor, with $[\text{Fe}/\text{H}] < -4$, which have not yet been found by extensive surveys of such stars to date (Beers 2000). This problem may be precluded if we consider the pre-enrichment of gas in a cosmological scale (e.g., Cen & Ostriker 1999).

is at work, HVCs would modify the long-term star formation history of the simulated disk at $0 \leq z < 1$.

Figure 5 shows the relation between ages and metallicities of the stars formed in the simulated Galaxy. As a natural result of chemical evolution inside clumps, more metal-rich stars tend to have younger ages. The excess of stars can be seen in the age between 9 and 10 Gyr, which corresponds to the epoch of starburst triggered by merging between two massive clumps at $z \sim 1.5$. Also, there is a large dispersion in metallicities for stars with given ages (e.g., metallicities range from -1.0 to 0.4 dex for stars with ages ~ 5 Gyr), in sharp contrast to the prediction of a simple, one-zone chemical evolution model. This dispersion in the relation between metallicities and ages is explained in the following way. First, chemical evolution proceeds independently in each clump having mutually different gaseous metallicity, so that the stars born in different clumps have different metallicities, even if they are born at the same epoch. Second, in contrast to a one-zone model, mixing of metals is incomplete, so that gaseous metallicity is made considerably inhomogeneous inside each clump.

The present numerical simulation as well as other chemodynamical models based on the standard CDM model (Steinmetz & Müller 1995; Bekki 2000; Bekki & Chiba 2000a) reveal that the number fraction of metal-poor disk stars with metallicities less than $0.25 Z_{\odot}$ (where Z_{\odot} is solar metallicity) is estimated to be $10 - 20$ %, which is still inconsistent with the observed value of 2 %. Thus, these CDM-based models encounter the so-called G-dwarf problem in the solar neighborhood (e.g., Thuan et al. 1975). We note that this failure is due principally to the adopted initial condition (i.e., isolated gaseous sphere) and that the problem may be solved by invoking the later accretion of gas-rich HVCs. The physical process related to the accretion of HVCs onto the Galactic disk and its role in solving the G-dwarf problem will be presented elsewhere.

Figure 6 and 7 present the final spatial distribution of the stars at $z = 0$, for a given metallicity and age range, respectively. It is clear that the distribution of more metal-poor (metal-rich) stars is likely to be more spherical (disky), which means that progenitor gas clouds for more metal-poor (metal-rich) stars experience less (more) amount of gaseous dissipation in the early dynamical evolution. Furthermore the distribution of older (younger) stars is likely to be more spherical (disky), which is a consequence of the process that old bulge and halo components are formed basically through merging between subgalactic clumps, whereas a young disk is formed from later gradual and dissipative gaseous accretion. It is also clear from these figures that the central bulge component contains old and metal-rich stars, though it emerges at moderate redshift ($z \sim 1.5$) after the major merging of two massive clumps: in the present hierarchical picture, a significant

fraction of stars that compose the present-day bulge are already formed at high redshifts ($z > 2$) within the central region of clumps. Thus, this suggests us that even if the Galactic bulge is observed to contain old and metal-rich stars (McWilliam & Rich 1994), it does *not* necessarily indicate that the bulge is formed *in situ* at high redshift. This aspect for the bulge formation was also emphasized by Noguchi (1999).

The disk component, on the other hand, is basically young and metal-rich compared with other spherical components, because the disk is formed by later accretion of enriched gas, which is tidally stripped from subgalactic clumps during their merging event. Furthermore the disk thickness is systematically smaller for more metal-rich stars, which suggests that gaseous dissipation plays an important role in determining the disk thickness. It is noted that the thickening of the forming disk is also driven by two-body scattering of disk stars by their interaction with rapidly moving high-mass dark matter particles (e.g., Steinmetz & Müller 1995). Here we are unable to separate between the so-called thick and thin disks owing to the resolution of the present simulation (~ 2 kpc, which is comparable to or larger than the characteristic thickness of both disk components). However, *if* the thicker disk obtained from our simulation with the age between 8 and 10 Gyr (corresponding to the lower middle panel in Figure 7) corresponds to the Galactic thick disk, Figure 7 implies that it is formed while surviving less massive clumps are still merging with the young Galaxy at the epoch of 8 – 10 Gyr. We also note that, from the lower middle panel of Figure 7, the morphology of the early Galaxy about 8 Gyr ago may have looked like a S0 galaxy or a disky elliptical galaxy, rather than currently seen – we here stress that not all of stars with the age between 8 – 10 Gyr have already assembled into the Galaxy 8 Gyr ago. This implies that some high redshift galaxies, morphologically classified as S0s, can be transformed to more late-type disk galaxies at lower redshift, owing to later gaseous infall and the resultant disk growth.

3.2. Halo properties

In the following, we focus on the results for the metal-poor stars with $[\text{Fe}/\text{H}] \leq -1.0$ that are expected to build up the present-day Galactic stellar halo.

3.2.1. Star formation history

Figure 8 shows the number fraction of the stars having older ages than a given age (cumulative age distribution), for the metallicity ranges of $[\text{Fe}/\text{H}] \leq -1.6$ (solid line) and

$-1.6 < [\text{Fe}/\text{H}] \leq -1.0$ (dotted line), respectively. In other words, the plot shows the number fraction of the stars which have already been formed by the given epoch. Since these metal-poor stars are considered to compose the present-day Galactic halo, this figure is expected to describe its star formation history. It follows that most of metal-poor stars ($\sim 80\%$) with $[\text{Fe}/\text{H}] \leq -1.6$ are already formed 10 Gyr ago ($z > 2$), thereby confirming that such stars are born initially inside subgalactic clumps at high redshifts. The figure also suggests that the time scale for the formation of old, metal-poor stars is of the order of a few Gyr, not 10^8 yr as was envisaged by ELS.

On the other hand, the stars with $-1.6 < [\text{Fe}/\text{H}] \leq -1.0$ still continuously form between 6 Gyr and 10 Gyr, though a significant fraction of them (42 %) have been already formed at $z > 2$. These relatively young, more metal-rich halo stars are formed from dissipative accretion of already enriched gas that was initially within subgalactic clumps but later stripped tidally during their merging event. This result suggests that some metal-poor halo stars with $-1.6 < [\text{Fe}/\text{H}] \leq -1.0$ show younger ages than those with $[\text{Fe}/\text{H}] \leq -1.6$. These young populations might show small abundance ratios such as $[\text{Mg}/\text{Fe}]$, compared with old populations with $[\text{Fe}/\text{H}] \leq -1.6$. It is interesting to explore if future observations reveal the systematic age difference between $[\text{Fe}/\text{H}] \leq -1.6$ and $-1.6 < [\text{Fe}/\text{H}] \leq -1.0$.

3.2.2. Morphology and structure

Figure 9 shows how the metal-poor halo populations with $[\text{Fe}/\text{H}] \leq -1.6$ are formed during the collapse of the Galaxy. Clearly, a large fraction of such stars ($\sim 50\%$) have already been formed inside small-scale density maxima at early epoch $z \gtrsim 2.6$. Then, the numerous small clumps, developed from these density maxima, merge or tidally interact with one another, and stars inside them are spread over the outer part of the halo. We note that these early processes proceed basically in a dissipationless way, because gas inside small clumps are quickly consumed by star formation or disrupted by tidal interaction. While these events take place, two massive clumps are developed by their gravity and spiral toward the inner part of the halo. These massive clumps, composed of both stars and gas, are then tidally disrupted during their strong interaction and merging ($z = 1.75$, and 1.28). Many metal-poor stars stripped by these processes are spread over the inner part of the forming Galaxy and build up the dense, inner part of the halo. To summarize, the halo formation involves dissipationless merging of many small clumps in its outer part and dissipative merging of two massive clumps in its inner part.

As is shown in Figure 10, the radial density distribution of the halo at $r \leq 20$ kpc is similar to the observed power-law, $\rho(r) \propto r^{-3.5}$, where r is the distance from the center

of the disk (Saha 1985; Hawkins 1984; Preston et al. 1991; Sommer-Larsen & Zhen 1990; CB). Figure 11 and 12 show the meridional distributions of the stars with $[\text{Fe}/\text{H}] \leq -1.6$ (left panels) and $-1.6 < [\text{Fe}/\text{H}] \leq -1.0$ (right panels) at two different redshifts, $z = 0$ (a) and 0.97 (b). It follows from the panels for $z = 0$ that the inner part of the halo is appreciably flattened, in particular, for stars with $-1.6 < [\text{Fe}/\text{H}] \leq -1.0$, whereas the outer part is more likely to be spherical. Also, we see the lack of stars along the polar axis. These simulated results are in good agreement with the observed dual nature of the stellar halo, characterized by an inner flattened part at $R \lesssim 15$ kpc and an outer spherical part (Hartwick 1987; Sommer-Larsen & Zhen 1990; Preston et al. 1991; Kinman et al. 1994; Layden 1995; CB). We note that this dual nature explains why studies of star counts generally yield an approximately spherical halo, whereas the local anisotropic velocities of the halo stars suggest a highly flattened system (Freeman 1987).

We now describe, in more detail, probable three physical processes involved in this duality of the halo.

The first is the difference in dynamical evolution of subgalactic clumps with different masses. Less massive and smaller clumps, that are formed from initial small-scale density fluctuations and do not grow steadily by merging with other clumps, are rather susceptible to destruction by strong tidal interaction and merging in the course of gravitational collapse of the Galaxy. The stars born inside such clumps are spread over the outer region of the proto-Galaxy after their destruction. Also, these less massive clumps are more likely to be completely destroyed *before* they spiral toward the central region of the proto-Galaxy, so that the tidally stripped stars are located in the outer region of the halo. Furthermore, since the tidal stripping occurs randomly among the clumps with variously different orbits, the disrupted stars also have mutually different orbits. This leads to the outer halo with spherical shape and with no systematic rotation, which is in good agreement with the reported properties of the outer halo (CB).

On the other hand, more massive clumps, that grow rapidly owing to multiple dissipative merging with other smaller clumps, gradually move toward the central region of the proto-Galaxy because of dynamical friction. These clumps are less likely to be completely destroyed by interaction with other small clumps. Since dynamical friction between clumps and background dark halo tends to circularize their orbits, they have a large amount of orbital angular momentum. Furthermore this dynamical friction makes the clumps approach to the Galactic plane (defined in the present epoch) before their merging. Finally, these massive clumps merge with each other in a considerably dissipative way owing to the large fraction of gas, and are consequently destroyed by the violent relaxation. Since most of the stars stripped from the clumps have orbital motions with a finite angular

momentum, similarly to the clumps themselves, the aftermath of this merging event shows a flattened halo with finite, prograde rotation. Thus, the present numerical model based on the standard CDM model suggests that both dissipationless merging in the outer part and dissipative merging in the inner part are responsible for the observed dual nature of the halo.

The second key process, which is only important for the inner halo, is the dynamical effect of the gradually growing disk on the halo structure (Binney & May 1986; Chiba & Beers 2001). As is shown in Figure 12, the spatial distribution of the stars with $-1.6 < [\text{Fe}/\text{H}] \leq -1.0$ for $R < 15$ kpc is more flattened at $z = 0$ than at $z = 0.97$. As the disk is not so developed at $z = 0.97$ (see Figure 2 and 3), this result suggests that the growth of the disk component due to later gaseous accretion compresses adiabatically the halo with an initially less flattened distribution, thereby leading to a more flattened halo in its inner part. This effect of adiabatic compression can be more clearly seen in the more metal-rich stars with $-1.6 < [\text{Fe}/\text{H}] \leq -1.0$ than $[\text{Fe}/\text{H}] \leq -1.6$, possibly because an ensemble of more metal-rich stars is systematically ‘colder’ owing to more dissipation of gas, before the disk growth.

The third process, which is also responsible for the formation of the inner halo alone, is drawn by comparing the spatial distributions of stars at the epoch of $z = 0$ with $z = 0.97$ in Figure 11. It appears that in the range of $10 \lesssim R \lesssim 20$ kpc near the plane, there are a larger number of stars with $-1.6 < [\text{Fe}/\text{H}] \leq -1.0$ at $z = 0$ than at $z = 0.97$. Furthermore, these stars at $z = 0$ clearly have a highly flattened distribution. These results suggest that such stars located in the range of $10 \lesssim R \lesssim 20$ kpc at the current epoch have been formed since $z = 0.97$ and that these newly born stars build up a flattened density distribution. The probable reason for its flattened distribution is that these stars are formed from later gaseous accretion onto the outer part of the disk and thus sustain a large amount of gaseous dissipation prior to their birth, as was envisaged by Chiba & Beers (2001). Such later formation of a highly flattened halo composed mostly of relatively young (8–10 Gyr) stars cannot be seen clearly for the more metal-poor stars with $[\text{Fe}/\text{H}] \leq -1.6$. This is consistent with the fact that most of stars with $[\text{Fe}/\text{H}] \leq -1.6$ are formed more than 10 Gyr ago (see Figure 8). Thus, we can conclude that the outer nearly spherical halo is formed by merging of less massive subgalactic clumps, whereas the inner flattened halo is formed by three different mechanisms: highly dissipative merging between more massive clumps, adiabatic compression due to secular and gradual disk growth, and later dissipative gaseous accretion onto the disk plane.

It should also be remarked that in all metallicity ranges and redshifts, there appears the lack of stars along the polar axis of the simulated halo. This was actually obtained

from kinematic analyses of nearby metal-poor stars (Sommer-Larsen & Zhen 1990; CB), but was attributed to the small probability that stars exploring near the polar axis are represented in the solar neighborhood. However, our model suggests that it is *real*. It is possibly due to the effect of dynamical friction between dark matter halo and subgalactic clumps: dynamical friction makes clumps approach to the disk plane, so that the spatial distribution of metal-poor stars, which are tidally stripped from these clumps, tend to avoid the region near the polar axis.

3.2.3. $[Fe/H]$ vs e relation

Figure 13 shows that there is no significant correlation between $[Fe/H]$ and e for the stars with $[Fe/H] \leq -0.6$, and that the existence of low eccentricity ($e < 0.4$), low metallicity ($[Fe/H] < -1$) stars is successfully reproduced in the present CDM model. This may be explained in a following manner. First, as ELS argued, the rapid contraction of a gravitational potential within a dynamical time ($\sim 10^8$ yr) results in the transformation of initially nearly circular (smaller e) orbits to very eccentric (larger e) ones. On the other hand, the eccentricities of the orbits remain basically unchanged if the contraction is slow enough ($\sim 10^9$ yr). In the present CDM model, the time scale for the contraction of the Galaxy is lengthened by the expanding background universe (the collapse time scale of a proto-galactic sphere with a turn-around radius of ~ 100 kpc is of the order of Gyr), so that the process of star formation mainly triggered by merging of small clumps is rather extended (~ 2 Gyr). Thus, the orbital eccentricities of the metal-poor stars, once formed, are not greatly influenced by the change of an overall gravitational potential of the Galaxy. Second, as we mentioned above, most of the metal-poor stars have been confined within the massive clumps, where their orbits are gradually circularized due to dissipative merging with smaller clumps and dynamical friction with the background dark halo. Thus, a finite fraction of the debris stars after the last merging event preserve the orbital angular momentum of the clumps. Both of these processes may give rise to the existence of low- e , low- $[Fe/H]$ stars in the simulated Galactic halo. Although the observational evidence of no significant correlation between metallicity and eccentricity in metal-poor halo stars of the Galaxy is suggested to conflict with ELS's monolithic scenario (CY), it has not been explicitly clarified whether this observational evidence is consistent with the merger picture that is originally proposed by SZ. Thus the present numerical study first demonstrates that the SZ picture is more plausible to explain the observed $[Fe/H]$ - e relation.

To be more quantitative, we plot, in Figure 14, the cumulative e distributions of the metal-poor stars with $[Fe/H] \leq -1.6$ (solid line) and $-1.6 < [Fe/H] \leq -1.0$ (dotted line).

For the halo component with $[\text{Fe}/\text{H}] \leq -1.6$, the fraction of the simulated low- e stars with $e < 0.4$ is about 0.17, which is in good agreement with the observational result of about 0.2 (CY; CB). Also, as is consistent with the observational result, the cumulative e distribution in the intermediate abundance range $-1.6 < [\text{Fe}/\text{H}] \leq -1.0$ is systematically larger than that for $[\text{Fe}/\text{H}] \leq -1.6$. The fraction of the simulated low- e stars with $e < 0.4$ in this abundance range (~ 0.45) is somewhat larger than the observation (~ 0.35), suggesting that the metal-weak thick disk component, which is emerged in this intermediate abundance range, is somewhat over-produced. Besides this small deviation from the observation, we conclude that the reported kinematic and chemical properties of the Galactic halo are basically understandable in the context of the CDM-based model for the Galaxy contraction.

3.2.4. V_ϕ vs $[\text{Fe}/\text{H}]$ relation

Mean metal abundance of stellar populations in each region of the Galaxy reflects at what rate star formation has proceeded, depending on the amount of gaseous dissipation. Also, mean azimuthal velocity ($\langle V_\phi \rangle$) of stellar populations reflects the loss of angular momentum (in the R -direction) before their birth, accompanied by gaseous dissipation. Although these considerations are not necessarily true if the Galaxy has been assembled from subgalactic clumps with their own formation histories, it might not be unreasonable to say that a relation between $[\text{Fe}/\text{H}]$ and $\langle V_\phi \rangle$ for an ensemble of stars tells us about (1) to what extent a subgalactic clump containing stars dissipates its kinetic energy owing to gaseous cooling and dynamical friction and (2) how the Galaxy dynamically evolves with time (e.g., Gilmore et al. 1990). Sandage & Fouts (1987) presented a linear relation between $[\text{Fe}/\text{H}]$ and $\langle V_\phi \rangle$, in favor of the ELS scenario, whereas subsequent researchers have disagreed with it (Norris 1986; Carney 1988; Morrison, Flynn, & Freeman 1990; CY; CB): the linear relation disappears at $[\text{Fe}/\text{H}] \lesssim -1.7$. Thus, it is intriguing to investigate what our numerical models, based on hierarchical clustering scenario, will provide on this relation.

Figure 15 shows $\langle V_\phi \rangle$ as a function of $[\text{Fe}/\text{H}]$. We have selected the stars with their apo-galactic distances ranging from 8.5 to 17.5 kpc, to avoid the contamination of bulge-like stars. Solid, dotted, and dashed lines denote the stars at all heights from the plane $|Z|$, $|Z| < 1$ kpc, and $|Z| > 1$ kpc, respectively. There are some notable features in this figure. First, the stars with $[\text{Fe}/\text{H}] < -2.2$ show a non-negative, finite amount of rotation, where $\langle V_\phi \rangle$ exhibits no systematic change with $[\text{Fe}/\text{H}]$. This implies that the clumps having such very metal-poor stars have not experienced large gaseous dissipation before the birth of stars; most of such stars are born inside yet small, metal-poor clumps that

are easily disrupted by merging/interaction with other clumps soon after their emergence. Second, the dependence of $\langle V_\phi \rangle$ on $[\text{Fe}/\text{H}]$ is discontinuous at around $[\text{Fe}/\text{H}] = -2.2$, where $\langle V_\phi \rangle$ is nearly zero or somewhat negative at any $|Z|$. As will be discussed later, we believe that this point at $[\text{Fe}/\text{H}] \sim -2.2$ is dynamically important in the history of the Galaxy formation, distinguishing the nearly linear increase of $\langle V_\phi \rangle$ with $[\text{Fe}/\text{H}]$ at $[\text{Fe}/\text{H}] > -2.2$ (as discussed below) and apparently no systematic change of $\langle V_\phi \rangle$ at less abundances. Third, at $[\text{Fe}/\text{H}] > -2.2$, $\langle V_\phi \rangle$ monotonously increases with increasing $[\text{Fe}/\text{H}]$. This highlights the importance of gaseous dissipation in this $\langle V_\phi \rangle$ vs $[\text{Fe}/\text{H}]$ relation as follows. The orbits of stars, initially confined inside a clump, are made circular having high angular momentum, if the host clump suffers from gaseous dissipation during its dynamical evolution. As the mass of the clump increases with time due to its gravity, it suffers from further dissipation induced by frequent merging with other clumps. As a consequence, more metal-rich stars that are formed in the later stage ought to have larger rotational velocity. Fourth, the stars at lower heights, $|Z|$, tend to have larger $\langle V_\phi \rangle$, implying that such stars suffer from a larger amount of gaseous dissipation prior to their birth. All of these features in the $\langle V_\phi \rangle$ vs $[\text{Fe}/\text{H}]$ relation are basically consistent with observations, although the inferred discontinuity in $\langle V_\phi \rangle$ is located at more metal-poor abundance than the reported value of ~ -1.7 dex. We here stress that these kinematical properties of the simulated metal-poor, old stars can be affected by long-term and somehow artificial two-body scattering resulting from the small number of particles adopted in the simulation.

Figure 16 shows the distributions of V_ϕ in a given metallicity range, for all stars (panel a) and stars at $|Z| < 2$ kpc (panel b). As is expected from the results shown in Figure 15, the very metal-poor range with $[\text{Fe}/\text{H}] \leq -2$ contains stars in both prograde and retrograde rotation; the former fraction is slightly larger. The larger fraction of prograde stars is more easily seen at $|Z| < 2$ kpc, which is consistent with the inferred vertical dependence of $\langle V_\phi \rangle$ in Figure 15. Also, the peak of the distribution shifts toward positive V_ϕ for more metal-rich ranges, as is also expected from the discussion given above. These properties of V_ϕ are also qualitatively in agreement with observations, except that the observations have revealed a finite fraction of stars in highly retrograde rotation, at $V_\phi < -100$ km s⁻¹. Absence of such stars in our results, based on simulation of an isolated system, suggests that later accretion of satellites plays a role in populating them.

3.2.5. Kinematic substructure in phase space

If the basic physics involved in the halo formation is the merging/accretion of subgalactic clumps, or equivalently dwarf-like satellites, and their resultant tidal disruption, it is of great importance to search for any signatures of fossil tidal streams in the halo, in order to reveal the orbital paths followed by the clumps that have already merged with the Galaxy long time ago, and thus to elucidate the merging history in the Galactic past (Lynden-Bell & Lynden-Bell 1995). There are a number of recent works addressing the nature of possible candidates of globular clusters, halo stars, and satellite galaxies with orbits tracing the fossil tidal streams (e.g., Majewski et al. 1994; Morrison et al. 2000). Also, since the phase mixing of stars composing tidal debris from the past mergers is expected to be incomplete (Helmi & White 1999), it is possible to find signatures of the past merging events in the form of kinematic substructures. Recently, Helmi et al. (1999) discovered a clear “fossil evidence” of the past merging events in the solar neighborhood by investigating the sample of metal-poor stars (see also CB). They identified a statistically significant clumping of stars in angular momentum diagram, L_z versus $L_\perp = (L_x^2 + L_y^2)^{1/2}$.

It is interesting to investigate whether such kinematic substructures are also evident in the present model in which merging between subgalactic clumps frequently occurs. Figure 17 shows the current distribution of the simulated stars with $[\text{Fe}/\text{H}] \leq -1.0$ in angular momentum diagram, L_z versus $L_\perp = (L_x^2 + L_y^2)^{1/2}$. We have selected stars at $6 < R < 11$ kpc and $|Z| < 2.5$ kpc, to mimic the plot of nearby stars within distance 2.5 kpc as adopted by Helmi et al. (1999) and CB. As is evident, there exists no clear clumping in angular momentum diagram. A possible reason for its absence is that since nearly all of merging events occurred before $z = 1$, any kinematic substructures may have already been smeared out owing to the violently relaxing gravitational potential, as is seen in Figure 1, 2, and 3. Also, it is possibly due to numerical effects in the present study, i.e. unrealistically short time scale of two-body relaxation, so that any substructures formed by merging/accretion disappear soon after their emergence in an artificial way.

We note that kinematic substructures are easily detectable, if some minor merging events occur only after the formation of the entire Galaxy structure has been completed. In such a later stage, the gravitational field is nearly steady, so that energy exchange between clumps and background is inefficient, compared to the stage of violent relaxation. This implies that the reported kinematic substructure may be caused by later accretion of a satellite, which is not taken into account in our simulations starting from the collapse of an isolated sphere. Thus our future large-scale simulations, which include both the kpc-scale dynamical evolution of the Galaxy and the 100kpc-scale later accretion processes, may well reproduce successfully the kinematical substructure discovered by Helmi et al. (1999).

3.2.6. *Metallicity distribution*

Figure 18 shows the metallicity distributions of the stars obtained from our simulation at $z = 0$. The upper panel is for the stars selected from the region $r > 4$ kpc and $|Z| > 4$ kpc, in order to isolate the halo component as possible. Its metallicity distribution has a peak at $[\text{Fe}/\text{H}] \sim -1.6$ and a long tail at lower abundances, in good agreement with observations (Laird et al. 1988; Ryan & Norris 1991). Such a distribution is basically unchanged even if we confine ourselves to the stars at larger $|Z|$. Ryan & Norris (1991) argued that the observed metallicity distribution of metal-poor stars is well fitted by the prediction of the mass loss modified model of simple chemical evolution (Hartwick 1976), with an effective yield of $\log_{10} y_{\text{eff}} = -1.6$. Our numerical model reveals the actual process of mass loss from the halo system, which reduces the yield in a simple model, in the framework of the CDM theory: gas in each of subgalactic clumps is immediately stripped after tidal disruption of clumps, so that star formation and chemical evolution inside clumps are ceased. As a consequence, the tidally stripped stars have more metal-poor abundances than predicted from a simple model.

In addition to this metal-poor component, we see a number of intermediate abundance stars ranging from -1.2 to -0.4 dex, reminiscent of the metallicity distribution of the Galactic thick disk (Wyse & Gilmore 1995). This implies that the scale height of the simulated disk component is larger than a characteristic value of $1 - 2$ kpc derived for the scale height of the thick disk (e.g., Yoshii, Ishida, & Stobie 1987; CY, see also Majewski 1993 for the argument of a much larger scale height). We note that this discrepancy is probably caused by the low spatial resolution of our simulation, ~ 2 kpc.

The lower panel in Figure 18 highlights the bulge-like central component, selected from the region $r < 4$ kpc. Its metallicity distribution is dominated by metal-rich stars, with a very long tail at lower abundances, which agrees well with the observed distribution in the Galactic bulge (McWilliam & Rich 1994; Ibata & Gilmore 1995).

3.2.7. *Age and metallicity gradients*

We plot, in Figure 19, the radial distributions of ages and metallicities of the simulated stars at $z = 0$. It follows that the metal-poor stars with $[\text{Fe}/\text{H}] \leq -1.6$ show virtually no remarkable age gradient. It is not unexpected, since most of stars with $[\text{Fe}/\text{H}] \leq -1.6$ are formed at high z and thus have uniformly old ages. Also, even if an age gradient is developed in the early stage of the halo formation, the later merging event between massive clumps smooth out the gradient owing to violent relaxation of the gravitational field. On the

other hand, a small but finite radial gradient for metallicity is seen ($\Delta[\text{Fe}/\text{H}]/\Delta r \simeq -0.012$ dex kpc $^{-1}$ for $0 \leq r \leq 25$ kpc), if *all* stars are concerned. The gradient is significantly reduced if we exclude the very metal-poor stars with $[\text{Fe}/\text{H}] < -4$. The existence of small metallicity gradient is caused by dissipative evolution of clumps. It is also caused by the mass-dependence of dynamical friction: more massive and thus more metal-rich clumps can approach more closely to the central region of the proto Galaxy, so that more metal-rich stars are spread there after tidal disruption.

4. Discussion

Although there have been many discussion on advantages and disadvantages of the ELS monolithic and SZ merger scenarios in explaining growing information on the detailed properties of the Galactic stellar halo, only a few studies are devoted, in the framework of the currently favored CDM scenario of galaxy formation. Thus, we mainly discuss about (1) success and failure of the hierarchical clustering scenario in explaining various aspects of the observed halo, and (2) how the scenario explains not only the stellar halo but also the bulge and disk components in the Galaxy.

4.1. The origin of the inner flat and outer spherical halo

It is unlikely that either the ELS or SZ scenario alone can fully explain the observed dual nature of the halo, showing an inner flattened part and outer spherical part (e.g., Freeman 1996; CB). One of the possible scenarios for the duality is to combine aspects of both the ELS and SZ scenarios, in which the outer halo is made up from merging and/or accretion of subgalactic objects, such as dwarf-type satellites, whereas the inner halo is formed from dissipative, ordered contraction on relatively short timescale (e.g., Sommer-Larsen & Zhen 1990; Norris 1994; Carney et al. 1996; Sommer-Larsen et al. 1997). This hybrid scenario is expected to explain the characteristic properties of the halo (Carney et al. 1996; CB). If it is the case, questions then arise: (1) what physical processes in the early dynamical evolution of the Galaxy are actually responsible for the hybrid formation picture and (2) how the origin of such two-fold collapse or merging can be explained by a more sophisticated and modern theory of galaxy formation. There have been, however, yet no theoretical studies which clearly answer these questions.

Our numerical studies have presented the detailed aspects of the above hybrid scenario and also other additional processes which give rise to the dual nature of the halo (§3.2.2).

Namely, we have demonstrated that the outer spherical halo is formed via essentially dissipationless merging of less massive and smaller subgalactic clumps, whereas the inner flattened halo is formed via three different mechanisms, i.e., dissipative merging between two massive clumps, adiabatic compression due to later disk growth, and rapid gaseous accretion onto the Galaxy at early epochs; all of these three mechanisms are, for the first time, consistently investigated in the present numerical study.

If the proposed halo formation is also the case in general disk galaxies with different Hubble types, the present study implies the following inter-relation between morphological type and halo structure in galaxies. First, a later type disk galaxy (more disk-dominated galaxy) may have a more flattened halo. As is demonstrated in our simulations, a bulge-to-disk ratio in a disk galaxy decreases with decreasing redshift owing to later gradual disk growth, whereas the halo structure becomes more and more flattened because of adiabatic compression of later disk growth. It is also remarked that in a hierarchical clustering scenario of galaxy formation, a smaller bulge-to-disk-ratio implies that a larger amount of gas has been accreted from the halo to disk, in a longer time-scale (e.g., Baugh et al. 1998). Thus, it is suggested that a later type disk galaxy, which is supposed to accrete a larger amount of gas, may yield a more flattened halo.

Second, an earlier type disk galaxy may have a denser halo, if such a galaxy are formed via more violent merging among more massive clumps, as is supposed for the formation of elliptical galaxies (e.g., Barnes 1992). Since dynamical friction is more effective for more massive clumps, they can approach more closely to the central region of the galaxy and then merge with one another there. Consequently, the aftermath of the merging may build up a bigger bulge. Since a larger number of stars are tidally stripped from these clumps and spread over a more inner part of the halo, the aftermath may build up a denser halo. Thus, a proto-galaxy having initially more massive clumps may lead to a bigger bulge and denser, perhaps more metal-rich halo. Katz (1992) has already pointed out that more substructures in a proto-galaxy results in the formation of a denser and bigger bulge. We thus suggest that such a mass-dependent evolution of subgalactic clumps in the early evolution of a disk galaxy can give rise to the correlation between bulge-to-disk ratio and halo density.

Although there are only a few observations for searching and studying structures of stellar halos in external disk galaxies (e.g., Morrison 1999), it is undoubtedly worthwhile to seek the predicted correlations between galactic morphologies and halo structures, especially with 10m class large telescopes.

4.2. Anisotropic nature of the halo velocity ellipsoid

Internal velocity distributions of the stellar halo also provide valuable information on the early dynamical history of the Galaxy. The local velocity field of metal-poor halo stars in the solar neighborhood, for which information on full space velocities are available, is characterized by a radially elongated velocity ellipsoid $(\sigma_R, \sigma_\phi, \sigma_Z) \simeq (141, 106, 94) \text{ km s}^{-1}$ (e.g., CB). Velocity distributions in other, more remote regions are yet uncertain because of the lack of accurate proper motion data, but the analysis of line-of-sight velocities combined with detailed modeling of the velocity fields allows to elucidate the global velocity distribution of the stellar halo. Based on this strategy, Sommer-Larsen et al. (1997) analyzed the sample of relatively bright, blue horizontal branch field stars and proposed that halo populations show distinct changes in their velocity ellipsoid as one moves from the inner to outer halo: in the inner part ($r \lesssim 10 \text{ kpc}$), the radial component of the velocity ellipsoid, σ_r , is systematically larger than the tangential component, σ_t ($\sigma_r \sim 140 \text{ km s}^{-1}$ and $\sigma_t = 90\text{--}100 \text{ km s}^{-1}$), whereas the outer halo at $r > 20 \text{ kpc}$ is tangentially anisotropic ($\sigma_r = 80\text{--}100 \text{ km s}^{-1}$ and $\sigma_t = 130\text{--}150 \text{ km s}^{-1}$).

We plot, in Figure 20, the radial dependence of σ_r and σ_t derived from the present simulation. We have selected the stars with $[\text{Fe}/\text{H}] \leq -1.0$ at $|Z| > 2 \text{ kpc}$ to isolate the halo component. Although the plot is not smooth due to the small number of available stellar particles, especially in the outer part ($R > 15 \text{ kpc}$), there is a signature of radially anisotropic velocity field in the inner part ($R < 12 \text{ kpc}$). The outer part appears to be tangentially anisotropic, but we admit that the result is not definite because of large errors in the calculation of velocity dispersion.

If the proposed radial dependence of σ_r and σ_t is the case, then what physical processes are responsible for such a change? The observed radial change of velocity ellipsoid may be explained via anisotropic, *dissipative* merging between protogalactic gas clouds in a collapsing galaxy (Sommer-Larsen & Christensen 1989; Theis 1997), as is described below. Protogalactic gas clouds which initially have radially eccentric orbits can plunge into the dense, inner region of the Galaxy and collide frequently with other clouds there. These clouds dissipate their kinetic energy and consequently never return to the radius from which their orbital motions started. The halo stars formed from such clouds would have rather radially eccentric orbits and continue to orbit only within the inner part of the Galaxy. On the other hand, protogalactic gas clouds which initially have less radially eccentric orbits (or more circular orbits) cannot plunge into the inner region and thus do not suffer from cloud-cloud collisions so frequently. These clouds therefore preserve less eccentric orbits and continue to locate in the outer part of the Galaxy. The orbits of halo stars formed from such clouds would be more circular. As a consequence, the inner halo

which is dominated by stars with radially eccentric orbits show more radially anisotropic velocity dispersion, whereas the outer halo containing stars with more circular orbits show tangentially anisotropic velocity dispersion.

An alternative picture is that the outer halo is more gradually formed from accretion of numerous fragments, such as satellite galaxies, having less eccentric orbits. To be more specific, most of stars now observed in the outer part of the halo are confined inside satellites, which are initially located at large distance from the Galaxy, having large orbital angular momentum, and the tidal disruption of such satellites occur at relatively later epoch, as in the case of the Sgr dwarf galaxy (Ibata, Gilmore, & Irwin 1984). Since the orbits of the stars somehow preserve less eccentric orbits of their progenitor satellites, the outer halo is made tangentially anisotropic.

We note that in the present simulation, the total number of subgalactic clumps are rather small owing to the small number of the adopted initial gaseous particles. Accordingly, *anisotropic* dissipative merging due to orbit-dependent collisions between clumps is suppressed, especially in the outer region of the system. Also, we have investigated an initially *isolated* system, without taking into account the effect of later accretion of satellites; merging and accretion events cease at relatively early epoch. Thus, it is yet unsettled from the present simulation, which picture described above is likely to explain the observed radial change of velocity dispersions. We are planning to revisit this issue, based on high-resolution simulations covering both 10 kpc-scale dynamical evolution of the Galaxy and 1 Mpc-scale merging history of dwarf-type galaxies in the forming Local Group.

4.3. The Galactic turning point

Many researchers have attempted to settle an issue as to how the rotational velocities of field halo stars, V_ϕ , change with their metallicities, since ELS’s work, showing larger V_ϕ for more metal-rich stars (e.g., Gilmore et al. 1990). Sandage and Fouts (1987) pointed out that there is a clear continuation of a *smooth* relation between $\langle V_\phi \rangle$ and $[\text{Fe}/\text{H}]$ and suggested that this correlation is an evidence supporting the monolithic collapse picture by ELS. On the other hand, using 1200 stars with $[\text{Fe}/\text{H}] \leq -0.6$, Norris (1986) argued that a continuously smooth change of $\langle V_\phi \rangle$ is not the case over an entire range of $[\text{Fe}/\text{H}]$: he found a sharp discontinuity at $[\text{Fe}/\text{H}] \sim -1.4$ below which there is no explicit dependence of $\langle V_\phi \rangle$ on $[\text{Fe}/\text{H}]$ (see also Norris & Ryan 1989; Beers & Sommer-Larsen 1995; CY; CB). He concluded that this result is consistent with the SZ picture that numerous protogalactic fragments merge with one another to form the Galaxy. Recent more detailed analysis by CB, using 1203 stars with revised information on their kinematics and metallicities, has

confirmed a clear discontinuity in the relation between $\langle V_\phi \rangle$ and $[\text{Fe}/\text{H}]$ at $[\text{Fe}/\text{H}] \sim -1.7$. CB also found, for stars with $-2.4 \leq [\text{Fe}/\text{H}] \leq -1.9$, a systematic decrease of $\langle V_\phi \rangle$ with increasing distance from the Galactic plane, $|Z|$. Based on these results, they concluded that (1) the rapid collapse picture by ELS is inconsistent with the discontinuous relation between $\langle V_\phi \rangle$ and $[\text{Fe}/\text{H}]$ and (2) totally chaotic merging in the SZ picture also has difficulties in explaining the vertical gradient of $\langle V_\phi \rangle$.

The present numerical simulations based on hierarchical clustering scenario have successfully reproduced *qualitatively* both the discontinuous change of $\langle V_\phi \rangle$ with $[\text{Fe}/\text{H}]$ and the vertical gradient of $\langle V_\phi \rangle$: dissipative merging of subgalactic clumps in the early epoch of galaxy formation ($[\text{Fe}/\text{H}] \leq -1.7$) and the subsequent gradual accretion of gas ($[\text{Fe}/\text{H}] > -1.7$) in the later stage give a plausible explanation for the observed properties of $\langle V_\phi \rangle$. The problem remained in our model is that the present simulation indicates the discontinuity at $[\text{Fe}/\text{H}] \sim -2.2$, which is systematically more metal-poor than the observed value of ~ -1.7 . Since we regard the point at $[\text{Fe}/\text{H}] \sim -1.7$ as a crucial epoch for understanding the Galaxy formation, as is described below, we will attempt to solve this discrepancy in our future work, by elaborating numerical models and investigating a full coverage of model parameters (Bekki & Chiba 2000b).

CB also showed that there is a concentration of high- e stars at $[\text{Fe}/\text{H}] \sim -1.7$, which gives rise to a nearly zero mean rotation of the stars at this metallicity. Except at this discontinuous point, $\langle V_\phi \rangle$ stays positive, 30–50 km s $^{-1}$, at $[\text{Fe}/\text{H}] < -1.7$, whereas at $[\text{Fe}/\text{H}] > -1.7$, $\langle V_\phi \rangle$ linearly increases with increasing $[\text{Fe}/\text{H}]$. As a consequence, there appears a hollow-like feature at $[\text{Fe}/\text{H}] \sim -1.7$ in the $\langle V_\phi \rangle$ vs $[\text{Fe}/\text{H}]$ relation (see Figure 3 in CB). It remains uncertain how this hollow-like feature, consisting of high- e stars, is created. In conjunction with this, it is equally important to explain the properties of $\langle V_\phi \rangle$ below and above $[\text{Fe}/\text{H}] \sim -1.7$, to elucidate physical processes involved in the formation of the halo and (thick) disk components, respectively. Thus, we believe that this hollow-like feature is a key to understanding how the stage of halo formation is discontinuously changed to that of disk formation.

Here we attempt to explain the origin of this discontinuous change of $\langle V_\phi \rangle$ and more details will be studied in Bekki & Chiba (2000b). Our models indicate that just at the epoch when the Galaxy as a whole has the mean metallicity of $[\text{Fe}/\text{H}] \sim -1.7$ (or the epoch when the Galaxy is dynamically dominated by massive clumps with $[\text{Fe}/\text{H}] = -1.7$), the last merging event between two massive clumps takes place. This merging event is totally violent and dissipative, as the mass ratio of these clumps is close to 1. Many of the stars after disruption preserve orbital angular momentum of clumps, thereby build up an inner halo with somewhat prograde rotation. On the other hand, strong gaseous

compression at the moment of merging give rise to newly born stars with $[\text{Fe}/\text{H}] \sim -1.7$. Such stars may have less amount of angular momentum because they are born within the strongly compressed region between both clumps. Furthermore, the orbits of such stars are randomized by violent relaxation in the final phase of merging of. Consequently, the orbital eccentricity of each of the stars becomes rather large. Thus, in this manner, we may be able to reproduce the observed discontinuous of $\langle V_\phi \rangle$ at $[\text{Fe}/\text{H}] \sim -1.7$: it is closely associated with the gaseous compression and violent relaxation due to the last merging event between subgalactic clumps. Since the basic process involved in the evolution of the Galaxy appears to be different between before and after this point, we would like to call it as *the Galactic turning point* in the Galaxy history.

The above picture provides the following further implications for the Galaxy formation (Bekki & Chiba 2000b). First, the Galactic bulge may have been formed at this epoch, owing to strong starburst associated with the last merging event. A large amount of compression and dissipation of gas at this point may induce an efficient radial inflow of gas and subsequently trigger strong starburst. The stars born by this process, which are well enriched because of rapid chemical evolution during starburst, may form a large fraction of the bulge. Some fraction of metal-poor, old stars, which are initially inside the clumps, are also expected to comprise the bulge. Therefore, if the bulge is formed in this manner, it is basically an old system having both metal-poor and metal-rich stars. Second, the formation of the halo component at the turning epoch may play a key role in the formation of the first *thin* disk, which is *not* the present-day thin disk as will be described later. This is inferred from the following. After the most part of the halo is formed, the gravitational potential stays nearly fixed, under which low density gas stripped during early merging events among numerous small clumps are fallen onto the equatorial plane, because there is no centrifugal barrier in this direction. This gradual accretion of gas may give rise to a thin disk in the equatorial plane.

4.4. Minor merging and thick disk formation

There are variously different scenarios for the formation of the thick disk component with a scale height of about 1 kpc (e.g., Gilmore et al. 1990; Majewski 1993). These include, (1) a rapid increase in the dissipation and star formation rate because of more rapid cooling of enriched gas with $[\text{Fe}/\text{H}] > -1$ (Wyse & Gilmore 1988), (2) violent dynamical heating of an early thin disk induced by minor satellite merging at high redshift (e.g., Quinn et al. 1993), (3) long-term kinematic diffusion of stars formed initially in a thin disk, and (4) direct satellite accretion of thick disk material (Statler 1989). We here focus on

the second minor merging scenario, because minor merging is expected to occur frequently in the hierarchical clustering scenario. In this scenario, the orbits of subgalactic clumps or satellites are circularized and are gradually fallen into the center of the disk, owing to dynamical friction and tidal force from the disk. The disk stars are heated dynamically by minor merging, and the aftermath is similar to the observed spatial structure and kinematics of the Galactic thick disk. The issues addressed here are (1) when such minor merging occurs in order to explain both the metallicity distribution and total mass of the thick disk, and (2) if the merger scenario explains the observed (small) metallicity gradient of the thick disk.

We here propose that if the minor merging between a first thin disk and a satellite galaxy (or subgalactic clump) occurs at $[\text{Fe}/\text{H}] \sim -0.6$, this scenario can settle the above two issues. After the bulge formation via the last merging event between massive clumps, the first thin disk begins to form and the chemical evolution proceeds, starting from an initial abundance of $[\text{Fe}/\text{H}] \sim -1.7$. If so, the stars formed inside the disk have metallicities larger than -1.7 . If the minor merging related to the thick disk formation occurs when the mean metallicity of stars reaches around -0.6 , the thick disk developed from dynamical heating is expected to contain stars with the metallicity ranging from -1.7 to -0.6 . The total mass of the thick disk may be determined by the total gas mass accumulated during the formation of the first thin disk. Furthermore, since both the first disk and the subgalactic clump have a large amount of gas, this minor merging occurs basically in a dissipative manner, where any spatial gradient in the metallicity of the thin disk remains preserved, in contrast to totally dissipationless merging (e.g., Bekki & Shioya 1998). Therefore, the vertical metallicity gradient in the first thin disk may be preserved in the thick disk.

Thus, this minor merger scenario may explain, without obvious difficulties, the observed properties of the Galactic thick disk. It is noted that starburst is triggered by minor merging (e.g., Mihos & Hernquist 1994). Furthermore, recent observational results on the relation between the vertical velocity dispersion of disk stars, σ_z , and their ages have demonstrated that there is a sudden increase of σ_z for disk stars with ages of 9 – 12 Gyr (Quillen & Garnett 2000). If such disk populations have the metallicity of ~ -0.6 and also show some evidence of the past starburst at $[\text{Fe}/\text{H}] = -0.6$, the validity of the minor scenario is greatly strengthened. In this regard, it is of interest to seek the more precise determination of the age-metallicity distribution of disk stars with the ages ranging from 9 to 12 Gyr and the mean metallicity of ~ -0.6 , to assess the minor merger scenario for the formation of the thick disk.

4.5. A rough sketch of the Galaxy formation

Based on the present numerical studies, we here summarize a possible scenario of the Galaxy formation in the framework of hierarchical merging of subgalactic clumps. To describe each evolutionary process step by step, we use the mean metallicity of gas inside the entire Galactic space as a rough indicator of clock.

4.5.1. $[Fe/H] < -1.7$

Just after the formation of numerous small clumps owing to the non-linear growth of initial small-scale density perturbations, these clumps tidally interact and merger with one another. Before the mean metallicity of gas reaches -1.7 dex, the stars inside these small clumps are tidally stripped during interaction and merging, and are subsequently spread over the outer part of the halo. This outer halo, consisting of old and metal-poor stars, has a spherical density distribution with no systematic rotation. Along with this process, two more massive clumps, having nearly equal masses, have been developed from multiple merging of small clumps, and chemical evolution proceeds inside them.

This picture for the formation of the outer halo is basically the same as the SZ scenario. The time scale involved in this process is more than 1 Gyr, which is slow compared with a typical free-fall time of 10^8 yr in the Galaxy, for the reason that gravitational collapse is delayed owing to the expansion of the background Universe.

4.5.2. $[Fe/H] \sim -1.7$

When the gaseous metallicity inside the two massive clumps reaches $[Fe/H] \sim -1.7$, they merge with each other and the aftermath after their disruption forms an inner part of the halo. During this merging event, strong gaseous compression and violent relaxation take place, leaving newly born stars with less amount of angular momentum. As a result, such numerous stars having metallicity $[Fe/H] \sim -1.7$ show high- e orbits and thus small mean rotation. Also, rapid radial infall of gas to the center of the system is induced by efficient dissipation, triggering starburst in a bulge-like component. The stars born by this starburst activity are well enriched, as the chemical evolution rapidly proceeds in this central component. If some globular clusters are associated with the clumps, they are also stripped from the clumps and may form the system of halo globular clusters having metal-poor stellar populations. These clusters may also have high e and small $\langle V_\phi \rangle$.

4.5.3. $-1.7 < [Fe/H] < -0.6$

Successive accretion of the surviving, small clumps onto the equatorial plane of the Galaxy continues, even after the end of the last merging event. Gas in these clumps is accumulated in the plane, thereby making up a thin disk. In addition, some more gas associated with HVCs may also accrete from outside and increase the mass of the disk. Star formation and chemical evolution give rise to enriched disk stars having large rotational velocity. As gaseous dissipation proceeds and thus drives a gradual accretion in the radial direction, more metal-rich stars are expected to rotate more rapidly, leading to the linear increase of $\langle V_\phi \rangle$ with $[Fe/H]$. We estimate the total mass of this first thin disk as $\sim 10\%$ of the mass of the present-day stellar system in the Galaxy ($\sim 6.0 \times 10^9 M_\odot$).

4.5.4. $[Fe/H] \sim -0.6$

When the mean metallicity of the thin disk reaches $[Fe/H] \sim -0.6$, one or some relatively massive satellites, having the mass of a few % of the present Galaxy and with high angular momentum, may slowly spiral toward the Galaxy. Dynamical friction and tidal force from the thin disk make the orbit of the satellite become more circular and approach to the disk plane. Then, the minor merging takes place, which results in the dynamical heating of the disk, preferentially in the Z direction. This minor merging thus develops the disk having a large scale height, perhaps comparable to the present-day thick disk. This disk component contains the stars with $-1.7 \lesssim [Fe/H] \lesssim -0.6$ originally included in the first thin disk, and also some more metal-rich stars born in the process of gaseous dissipation during merging. Gaseous dissipation also induces radial flow of gas to the central region and triggers nuclear starburst, so that both the mass and metallicity of the bulge component are increased.

If the sinking satellite contains globular clusters, they are tidally stripped, and form the system of clusters near the plane, which may correspond to the observed disk clusters in the Galaxy. Since the orbital angular momentum of the satellite is transferred to the stripped globular clusters, the cluster system developed after this minor merging event shows a net rotation, in contrast to the halo clusters.

4.5.5. $[Fe/H] > -0.6$

Along with or after the formation of the thick disk, the replenishment of gas near the disk plane may continue, in the form of cooling flow from rarefied gas in the halo or HVCs

from outside, thereby making up another thin disk component. Since this accretion process progresses in a quiescent manner, the disk remains thin. As the stars in this thin disk have been formed from a continuously replenished gas, their metallicity distribution may be exempted from the so-called G dwarf problem. This disk component may correspond to the present-day thin disk with a scale height of ~ 350 pc.

4.6. Future work: Extragalactic halo astronomy

It is intriguing to examine whether our models aimed at understanding the Galactic stellar halo are also applied to external disk galaxies. For instance, the following questions are immediately concerned: (1) Are there any difference in dynamical and chemical properties of stellar halo components among disk galaxies with different Hubble types? (2) Are there any physical correlation between, for example, bulge size and mean halo density? (3) How can merging processes of subgalactic clumps control the final dynamical and chemical properties of stellar halos in other galaxies? We believe that extensive observational studies of external stellar halos to answer these questions will shed new insight into the formation of general disk galaxies, in addition to further information on the Galaxy as provided by next generation astrometric satellites (e.g., *FAME* and *GAIA*). Also, further modeling of a halo component over a full range of model parameters (Bekki & Chiba 2000b) is important to understand how a variety of halos are developed in other disk galaxies.

Here, we point out the following two aspects to be investigated thoroughly, as a possible route to the general picture for the halo formation.

One is to extract the detailed projected light distributions of stellar halos in external disk galaxies. In the case of M31’s stellar halo, its surface luminosity distribution follows the so-called $R^{1/4}$ law, where R is the projected distance from the center (e.g., Freeman 1999). This is in contrast to the surface density distribution expected from the power-law volume density of $\rho(r) \sim r^{-3.5}$ in the Galaxy. Furthermore, it is suggested that the mean density of M31’s stellar halo is ten times higher than that of the Galactic halo (Guhathakurta, Reitzel, & Grebel 2000). These observed difference between the Galactic and M31’s halos may reflect the different formation history of halos in these galaxies. In addition, Morrison (1999) suggested a marginal evidence that there is a variety of structures in the stellar halos of external edge-on disk galaxies with different Hubble types. In this regard, we note that our preliminary calculations, as will be reported in our next paper, suggest that final structures of stellar halos depend sensitively on initial conditions of protogalaxies, such as spin parameters and amplitudes of CDM perturbations (Bekki & Chiba 2000b). Thus, it is of great interest to conduct further and more detailed observations of stellar halos in many

disk galaxies and compare with such theoretical results, in order to clarify the formation process of the stellar halo as well as the origin of the Hubble sequence. Such studies should be eagerly pursued with 10m class telescopes, such as *SUBARU* and *VLT*, taking advantage of their ability to detect faint images. We believe that extracting global distributions of stellar halos and also some spatial substructures using large telescopes will shed new insight into our understanding of galaxy formation.

The other is to determine the color distributions of stellar halos with different Hubble types, in addition to the light distributions. These information will provide us with both the initial mass function (IMF) in the formation of the stellar halo and the nature of halo populations as indicative of their age and metallicity distributions. Recent observational studies on the photometric properties of NGC 5907 have suggested that peculiar colors in its halo component imply the different shape of IMF as well as the different lower and upper mass limits in IMF, from the widely accepted Salpeter IMF (e.g., Zepf et al. 2000). It is thus important to conduct further observations of color distributions, to elucidate any differences in the inferred IMF among disk galaxies with different Hubble types and any evidence of the relation between the shape of IMF and the structural parameters of disks such as bulge-to-disk ratio. It is similarly important to elaborate chemodynamical models for the formation of stellar halos, taking into account evolutionary population synthesis. The detailed comparison between such models and observations will allow us to clarify any relations between early dynamical processes and photometric properties of halos, so that we will be able to obtain a more advanced picture on the origin of the Hubble sequence.

4.7. Limitations of the present model

In the present study, we have adopted an isolated rotating sphere superposed by small-scale density fluctuations for the investigation of the halo formation. Owing to this rather specific initial condition of the proto-Galaxy, both effects of satellite (or gaseous) accretion onto the Galaxy and major merging at lower redshifts are suppressed in the present simulations. Since these physical processes may affect the formation histories of the stellar halo, it is worthwhile to consider how these processes affect our results. We discuss below three possible aspects involved in later accretion or merging events onto the simulated isolated system, and firmer predictions await planned, more extended simulations.

First, later accretion of dwarf-type satellites can change the derived halo structure, in particular the slope of the density profile. Stellar components of satellites, which are tidally disrupted by the Galaxy at low redshifts, can be dispersed into the (mainly) outer part of the Galaxy and thus add up stars there. The amount of the change in the density

profile of the halo depends on the detailed accretion process of satellites, e.g., how closely satellites can approach the inner part of the Galaxy before their tidal disruption. Second, such later accretion processes can form a statistically significant clumping of stars in angular momentum diagram, L_z versus $L_\perp = (L_x^2 + L_y^2)^{1/2}$, as was discovered by Helmi et al. (1999) in the solar neighborhood. Third, the time evolution of the bulge-to-disk-ratio discussed here can be modified if the effect of later accretion or merging onto the Galaxy is taken into account. Such events can rapidly increase the bulge-to-disk-ratio at low redshifts, because very efficient radial transfer of gas resulted from merging can trigger the nuclear starbursts that eventually form young bulge components, and because sinking massive satellites which reach the central region of the Galaxy can add up stars in the bulge.

5. Conclusions

We have performed numerical simulations for the formation of the Galactic stellar halo, based on the currently favored CDM theory of galaxy formation. The main results are summarized as follows.

(1) Basic physical processes involved in the formation of the stellar halo are described by both dissipative and dissipationless merging of subgalactic clumps and their tidal disruption in the course of gravitational contraction of the Galaxy. A large fraction of metal-poor stars ($\sim 50\%$), making up the present-day halo, are already formed at $z > 2.6$, inside the clumps which are developed from small-scale CDM density perturbations, and are then tidally stripped from the clumps by successive merging and spread over the halo at $1.5 < z < 3.0$. Although these halo populations are generally old, the formation of the entire halo structure is relatively recent, at $z \sim 1.5$.

(2) The radial density profile of the simulated halo is similar to the observed power-law form of $\rho(r) \sim r^{-3.5}$, implying that hierarchical merging of clumps is also responsible for the characteristic radial distribution of halo stars. We also see the lack of the simulated stars along the polar axis, which reflects the anisotropic effect of dynamical friction on the orbital motions of clumps.

(3) Our numerical model successfully reproduces the observed metallicity distributions of the halo and also bulge components. The simulated stars with $[\text{Fe}/\text{H}] \leq -1.6$ show virtually no radial gradient for stellar ages, because the intrinsic age spread among such stars is small and also the violent relaxation at the epoch of the last merging event between two massive clumps smoothes out any gradients. A small radial gradient is seen for stellar metallicities, in particular, in the inner region of the halo. This may reflect the dissipative

process of gas during the merging among clumps.

(4) The inner flattened and outer spherical halo is successfully reproduced qualitatively by the present model, based on the hierarchical clustering scenario. The outer spherical halo is formed via essentially dissipationless merging of less massive and smaller subgalactic clumps whereas the inner flattened one is formed via three different mechanisms, i.e., dissipative merging between more massive clumps, adiabatic compression due to later disk growth, and gaseous accretion onto the equatorial plane.

(5) For the simulated stars with $[\text{Fe}/\text{H}] \leq -1.0$, there is no strong correlation between metal abundances and orbital eccentricities, in good agreement with the recent observations. Moreover, the observed fraction of the low-eccentric stars is reproduced correctly for $[\text{Fe}/\text{H}] \leq -1.6$ and approximately for the intermediate abundance range of $-1.6 < [\text{Fe}/\text{H}] \leq -1.0$.

(6) The simulated stars with $[\text{Fe}/\text{H}] \leq -2.2$ show a small systematic rotation without explicit dependence on $[\text{Fe}/\text{H}]$, whereas the stars with higher metallicities show the linear increase of $\langle V_\phi \rangle$ with increasing $[\text{Fe}/\text{H}]$. These properties of $\langle V_\phi \rangle$ are generally in agreement with observations, although the observed $\langle V_\phi \rangle$ turns to increase with $[\text{Fe}/\text{H}]$ at somewhat higher $[\text{Fe}/\text{H}]$. Also, as is deduced from the observation, the simulated stars at lower heights from the plane, $|Z|$, show systematically larger $\langle V_\phi \rangle$.

(7) We have not found any clear clumping of simulated metal-poor stars in angular momentum space at $z = 0$, though merging of subgalactic clumps plays a decisive role in the formation of the halo. A possible reason for its absence may be due to either numerical effects such as unrealistically short time scale of two-body relaxation or our specific initial condition of an isolated protogalaxy, which neglects later accretion of satellite galaxies.

Based on these results, we have discussed how early processes of both dissipationless and dissipative merging of subgalactic clumps can reproduce, plausibly and consistently, the recent observational results on the Galactic halo. Also, we have presented a possible scenario for the formation of the entire Galaxy structure, including the stellar halo, bulge, and disk components. It has also been remarked that further observational studies of faint halo components in external disk galaxies, using 10m class large telescopes, will provide us with invaluable information on the origin of the Hubble sequence in the context of hierarchical clustering scenario of galaxy formation.

We are grateful to the anonymous referee for valuable comments, which contribute to improve the present paper. K.B. acknowledges the Large Australian Research Council (ARC). We are grateful to Edmund Bertschinger for allowing us to use the COSMICS (Cosmological Initial Conditions and Microwave Anisotropy Codes), which is a package of

fortran programs for generating Gaussian random initial conditions for nonlinear structure formation simulations.

REFERENCES

- Barnes, J. E. 1992, *ApJ*, 393, 484
- Baugh, C. M., Cole, S., Frenk, C. S., & Lacey, C. G. 1998, *ApJ*, 498, 504
- Beers, T. C. 2000, in *The First Stars*, ed. A. Weiss, T. Abel, & V. Hill (Berlin: Springer-Verlag), 3
- Beers, T. C., & Sommer-Larsen, J. 1995, *ApJS*, 96, 175
- Beers, T. C., Chiba, M., Yoshii, Y., Platais, I., Hanson, R. B., Fuchs, B., & Rossi, S. 2000, *AJ*, 119, 2866
- Bekki, K. 1998, *ApJ*, 502, L133
- Bekki, K. 2000, in *The First Stars*, ed. A. Weiss, T. Abel, & V. Hill (Berlin: Springer-Verlag), 206
- Bekki, K., & Chiba, M. 2000a, *ApJ*, 534, L89
- Bekki, K., & Chiba, M. 2000b, in preparation
- Bekki, K., & Shioya, Y. 1998, *ApJ*, 497, 108
- Bertschinger, E. 1995, astro-ph/9506070
- Binney, J., & May, A. 1986, *MNRAS*, 218, 743
- Blitz, L., Spergel, D. N., Teuben, P. J., Hartmann, D., & Burton, W. B. 1999, *ApJ*, 514, 818
- Carney, B. W. 1988, in *IAU Symp. 126, The Harlow Shapley Symposium on Globular Clusters Systems in Galaxies*, ed. J. E. Grindlay & A. G. D. Philip (Dordrecht: Kluwer), 133
- Carney, B. W., Aguilar, L., Latham, D. W., & Laird, J. B. 1990, *AJ*, 99, 201
- Carney, B. W., Laird, J. B., Latham, D. W., & Aguilar, L. A. 1996, *AJ*, 112, 668
- Cen, R., & Ostriker, J. P. 1999, *ApJ*, 519, L109
- Chiba, M., & Yoshii, Y. 1998, *AJ*, 115, 168 (CY)
- Chiba, M., & Beers, T. C. 2000, *AJ*, 119, 2843 (CB)

- Chiba, M., & Beers, T. C. 2001, *ApJ*, 549, 325
- Combes, F., & Gerin, M. 1985, *A&A*, 150, 327
- Côte, P., Marzke, R. O., West, M. J., & Minniti, D. 2000, *ApJ*, 533, 869
- Eggen, O. J., Lynden-Bell, D., & Sandage, A. R. 1962, *ApJ*, 136, 748 (ELS)
- Flynn, C., Sommer-Larsen, J., & Christensen, P. 1996, *MNRAS*, 281, 1027
- Freeman, K. C. 1987, *ARA&A*, 25, 603
- Freeman, K. C. 1996, in *Formation of the Galactic Halo Inside and Out*, ASP Conference Series, eds. H. Morrison & A. Sarajedini (San Francisco: ASP), 3
- Freeman, K. C. 1999, in *The Third Stromlo Symposium: The Galactic Halo*, ASP Conference Series, eds. B. K. Gibson, T. S. Axelrod, & M. E. Putman (San Francisco: ASP), 167
- Gilmore, G., King, I., & van der Kruit, P. C. 1990, *The Milky Way as a Galaxy*, 19th Advanced Course of the Swiss Society of Astrophysics and Astronomy, eds. R. Buser, & I. King (Mill Valley, CA: Univ. Sci.)
- Guhathakurta, P., Reitzel, D. B., & Grebel, E. K. 2000, preprint (astro-ph/0004371)
- Hartwick, F. D. A. 1976, *ApJ*, 209, 418
- Hartwick, F. D. A. 1987, in *the Galaxy*, eds. G. Gilmore & B. Carswell (Cambridge: Cambridge Univ. Press), 281
- Hawkins, M. R. S. 1984, *MNRAS*, 206, 433
- Helmi, A., & White, S. D. M. 1999, *MNRAS*, 307, 495
- Helmi, A., White, S. D. M., de Zeeuw, P. T., & Zhao, H. S. 1999, *Nature*, 402, 53
- Ibata, R. A., Gilmore, G., & Irwin, M. J. 1994, *Nature*, 370, 194
- Ibata, R. A., & Gilmore, G. 1995, *MNRAS*, 275, 605
- Johnston, K. V., Spergel, D. N., & Hernquist, L. 1995, *ApJ*, 451, 598
- Kamionkowski, M., & Liddle, A. R. 1999, preprint (astro-ph/9911103)
- Katz, N. 1992, *ApJ*, 391, 502

- Katz, N., & Gunn, J. E. 1991, *ApJ*, 377, 365
- Kauffmann, G., White, S. D. M., & Guiderdoni, B. 1993, *MNRAS*, 264, 201
- Kinman, T. D., Suntzeff, N. B., & Kraft, R. P. 1994, *AJ*, 108, 1722
- Klypin, A., Kravtsov, A. V., Valenzuela, O., & Prada, F. 1999, *ApJ*, 522, 82
- Laird, J. B., Rupen, M. P., Carney, B. W., & Latham, D. W. 1988, *AJ*, 96, 1908
- Larson, R. B. 1974, *MNRAS*, 166, 585
- Layden, A. C. 1995, *AJ*, 110, 2288
- Lynden-Bell, D., & Lynden-Bell, R. M. 1995, *MNRAS*, 275, 429
- Ma, C.-P., & Bertschinger, E. 1995, *ApJ*, 455, 7
- Mihos, J. C., & Hernquist, L. 1994, *ApJ*, 425, 13L
- Majewski, S. R. 1993, *ARA&A*, 31, 575
- Majewski, S. R., Munn, J. A., & Hawley, S. L. 1994, *ApJ*, 427, L37
- McKee, C. F., & Ostriker, J. P. 1977, *ApJ*, 218, 148
- McWilliam, A., & Rich, R. M. 1994, *ApJS*, 91, 749
- Moore, B., Ghigna, S., Governato, F., Lake, G., Quinn, T., Stadel, J. 1999, *ApJ*, 524, L19
- Morrison, H. L. 1999, in *The Third Stromlo Symposium: The Galactic Halo*, ASP Conference Series, eds. B. K. Gibson, T. S. Axelrod, & M. E. Putman (San Francisco: ASP), 174
- Morrison, H., Mateo, M., Olszewski, E. W., Harding, P., Dohm-Palmer, R. C., Freeman, K. C., Norris, J. E., Morita, M. 2000, *AJ*, 119, 2254
- Noguchi, M. 1999, *ApJ*, 514, 77
- Norris, J. E. 1986, *ApJS*, 61, 667
- Norris, J. E. 1994, *ApJ*, 431, 645
- Norris, J. E., & Ryan, S. G. 1991, *ApJ*, 380, 403
- Norris, J. E., Bessell, M. S., & Pickles, A. J. 1985, *ApJS*, 58, 463

- Peacock, J. A. 1999, *Cosmological Physics* (Cambridge: Cambridge University Press)
- Preston, G. W., Shectman, S. A., & Beers, T. C. 1991, *ApJ*, 375, 121
- Quillen, A. C., & Garnett, D. R. 2000, preprint (astr-ph/0004210)
- Quinn, P. J., Hernquist, L., & Fullagar, D. P. 1993, *ApJ*, 403, 74
- Roberts, W. W., & Hausman, M. A. 1984, *ApJ*, 277, 744
- Ryan, S. G., & Norris, J. E. 1991, *AJ*, 101, 1865
- Saha, A. 1985, *ApJ*, 289, 310
- Sandage, A., & Fouts, G. 1987, *AJ*, 93, 74
- Schmidt, M. 1959, *ApJ*, 344, 685
- Schwarz, M. P. 1981, *ApJ*, 247, 77
- Searle, L. & Zinn, R. 1978, *ApJ*, 225, 357 (SZ)
- Shlosman, I., & Noguchi, M. 1993, *ApJ*, 414, 474
- Somerville, R. S., & Primack, J. R. 1999, *MNRAS*, 310, 1087
- Sommer-Larsen, J., & Christensen, P. R., 1989, *MNRAS*, 239, 441
- Sommer-Larsen, J., & Zhen, C., 1990, *MNRAS*, 242, 10
- Sommer-Larsen, J., Beers, T. C., Flynn, C., Wilhelm, R., & Christensen, P. R., 1997 *ApJ*, 481, 775
- Spergel, D. N., & Steinhardt, P. J. 2000, *Phys. Rev. Lett.*, 84, 3760
- Statler, T. S. 1989, *ApJ*, 344, 217
- Steinmetz, M., & Müller, E. 1995, *MNRAS*, 276, 549
- Steinmetz, M., & Navarro, J. F. 1999, *ApJ*, 497, 108
- Sugimoto, D., Chikada, Y., Makino, J., Ito, T., Ebisuzaki, T., & Umemura, M. 1990, *Nature*, 345, 33
- Theis, C. 1997, in *ASP Conf. Ser. 112, The History of the Milky Way and Its Satellite System*, ed. A. Burkert, D. H. Hartmann, & S. A. Majewski (San Francisco: ASP), 35

- Thuan, T. X., Hart, M. H., & Ostriker, J. P. 1975, *ApJ*, 201, 756
- Urban, S. E., Corbin, T. E., Wycoff, G. L., Morton, J. C., Jackson, E. S., Zacharias, M. I., & Hall, D. M. 1998, *AJ*, 115, 1212
- van den Bergh, S. 1996, *PASP*, 108, 986
- White, S. D. M., & Rees, M. J. 1978, *MNRAS*, 183, 341
- Wyse, R. F., & Gilmore, G. 1988, *AJ*, 95, 1404
- Wyse, R. F., & Gilmore, G. 1995, *AJ*, 110, 2771
- Yoshii, Y., & Saio, H. 1979, *PASJ*, 31, 339
- Yoshii, Y., Ishida, K., & Stobie, R. S. 1987, *AJ*, 93, 323
- Zepf, S. E., Liu, M. C., Marleau, F. R., Sackett, P. D., & Graham, J. R. 2000, *AJ*, 119, 1701

Fig. 1.— Distribution of dark matter particles of the forming Galaxy projected onto the x - z plane, at each of redshifts indicated in the upper left corner of each panel. Each frame measures 176 kpc on a side.

Fig. 2.— The same as Figure 1 but for gaseous particles.

Fig. 3.— The same as Figure 1 but for stellar particles formed from gas.

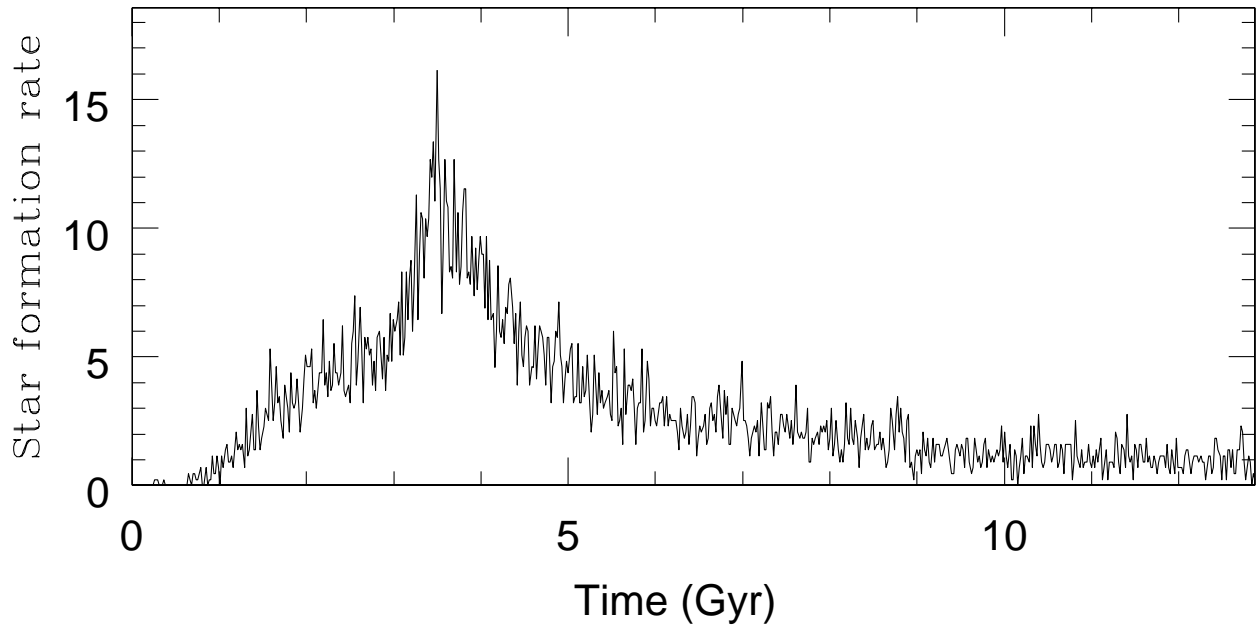


Fig. 4.— The star formation history of the present model in units of $M_{\odot} \text{ yr}^{-1}$.

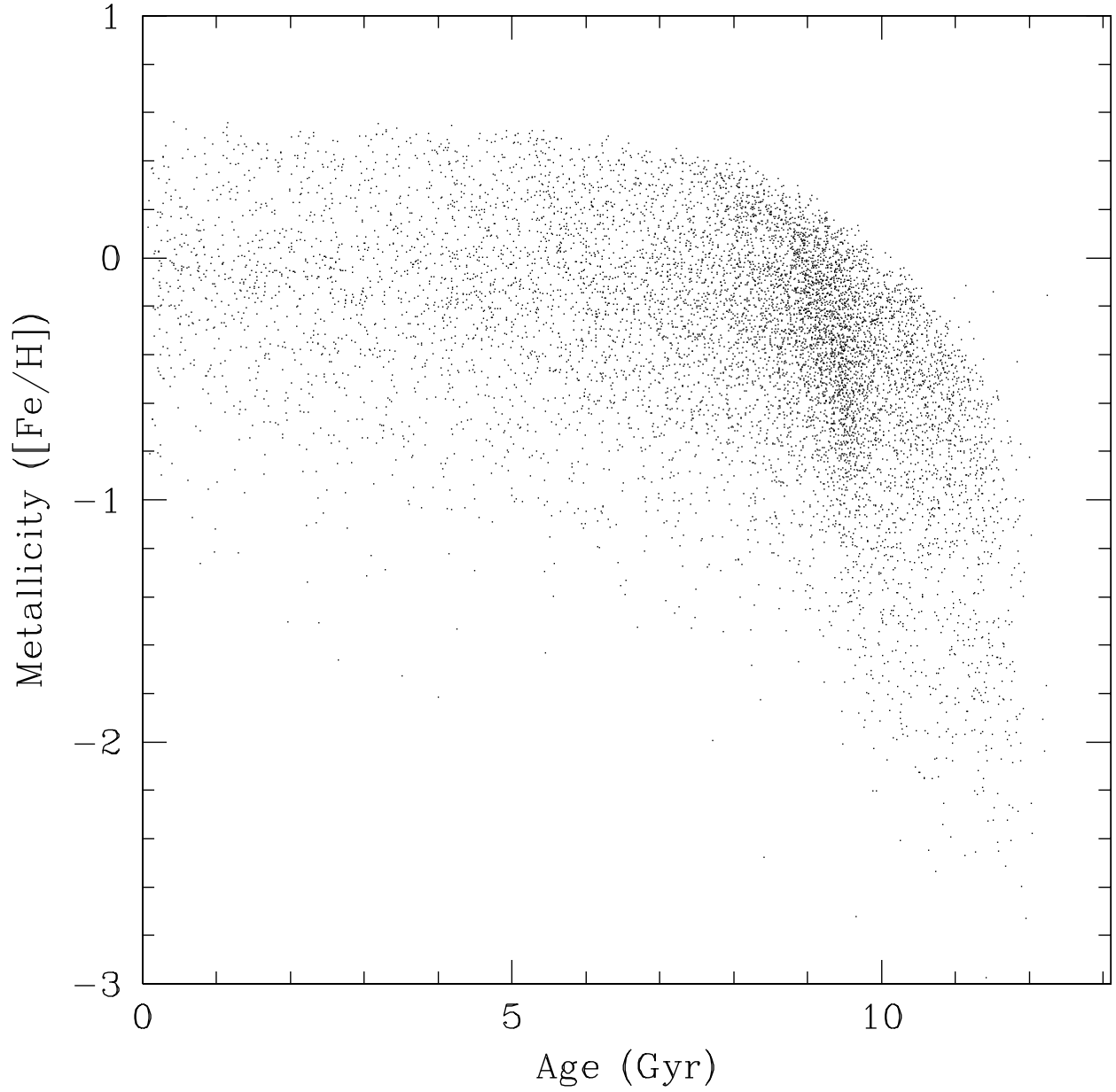


Fig. 5.— Age-metallicity diagram of the stars in our simulation. Note that there is a rather large dispersion in metallicities for a given age.

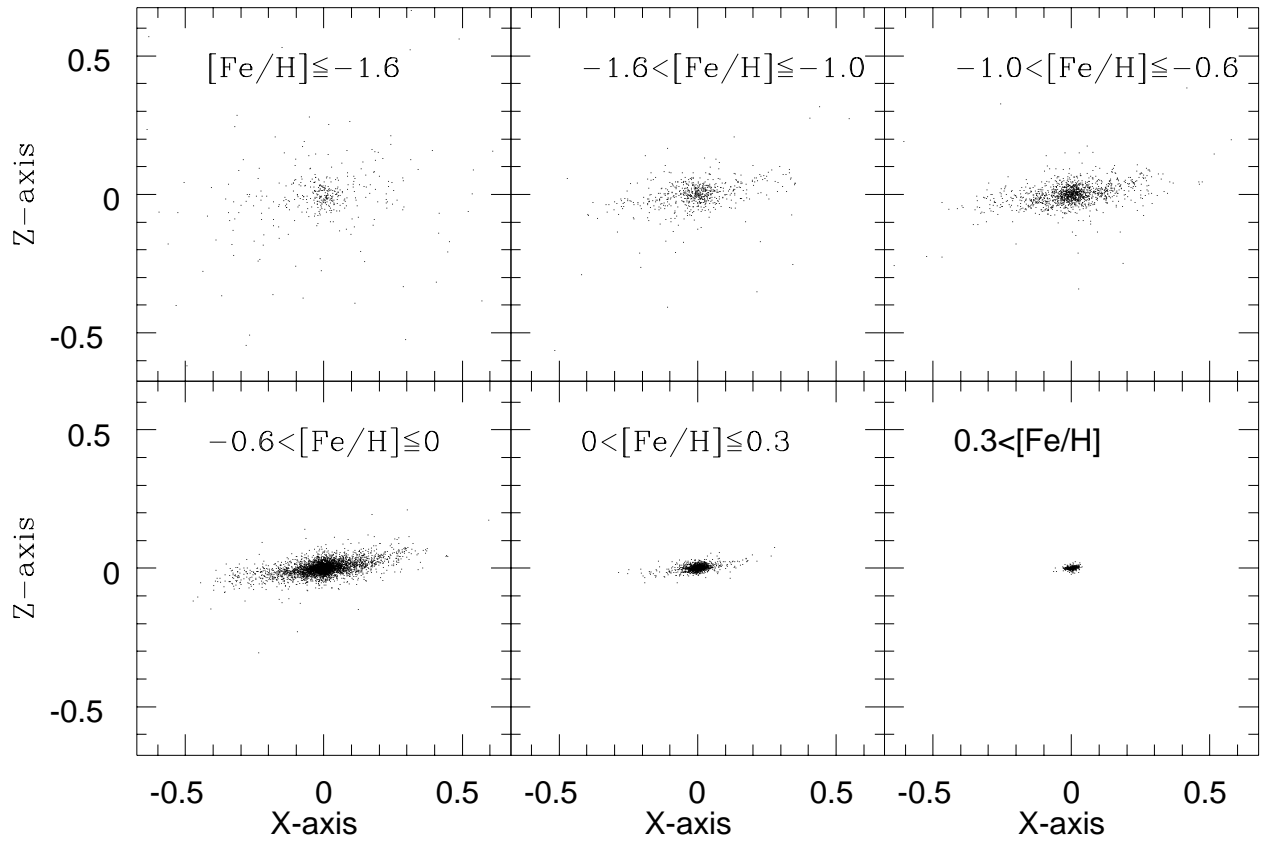


Fig. 6.— Final distribution of the stars for a given metallicity range, projected onto the x - z plane at $z = 0$ ($T = 13$ Gyr). The metallicity range is indicated in each panel. Each frame measures 58.5 kpc on a side.

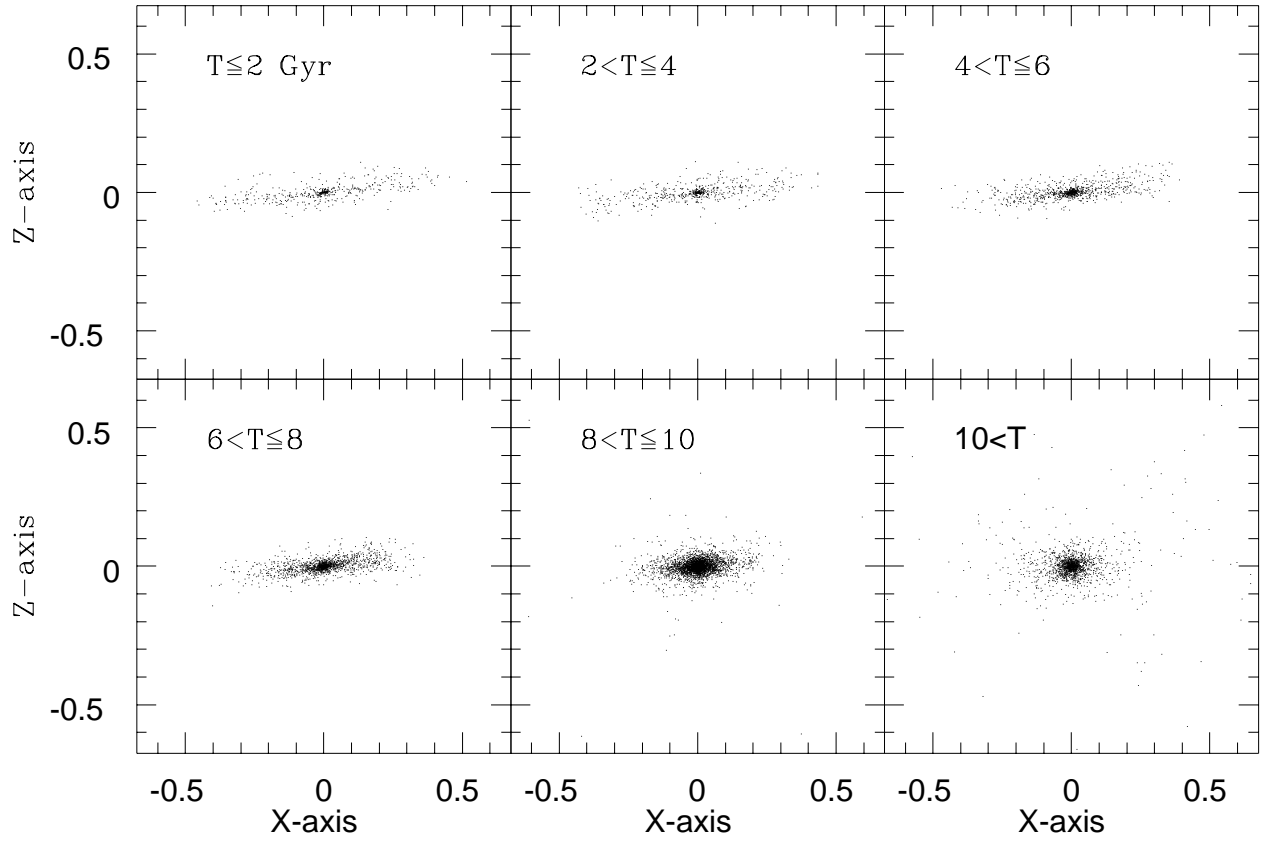


Fig. 7.— Final distribution of the stars for a given age range, projected onto the x - z plane at $z = 0$ ($T = 13$ Gyr). The age range is indicated in each panel. Each frame measures 58.5 kpc on a side.

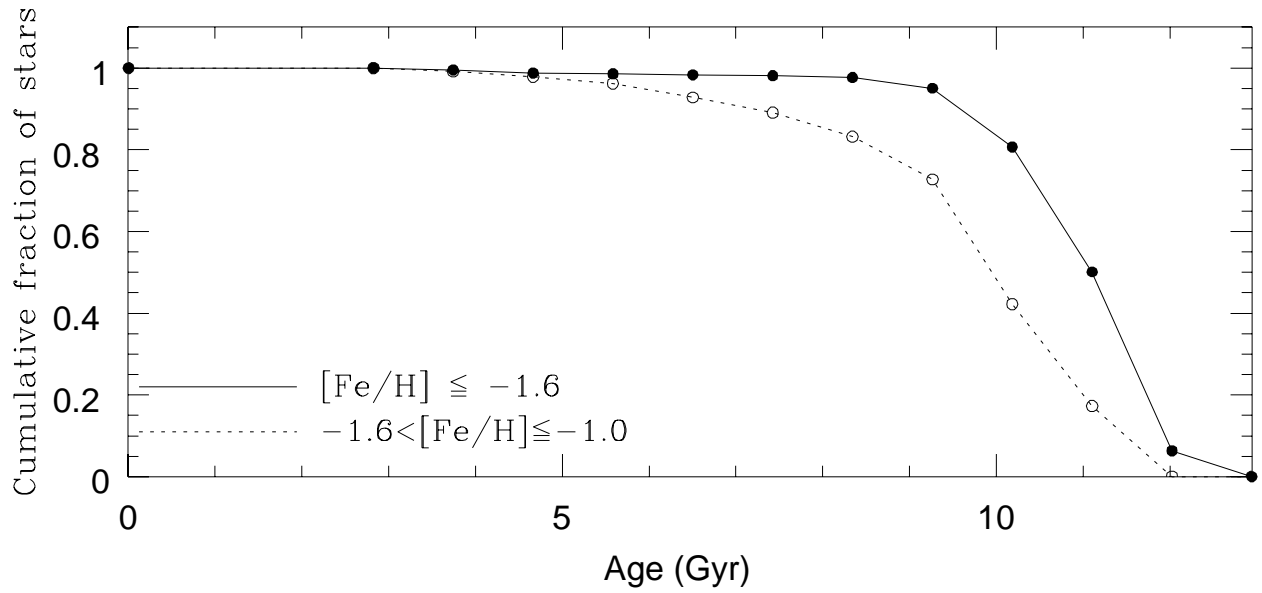


Fig. 8.— Number fraction of the stars having older ages than a given age (or cumulative age distribution), for the metallicity ranges of $[\text{Fe}/\text{H}] \leq -1.6$ (solid line) and $-1.6 < [\text{Fe}/\text{H}] \leq -1.0$ (dotted line), respectively. This figure also denotes the number fraction of the stars which have already been formed by the given epoch.

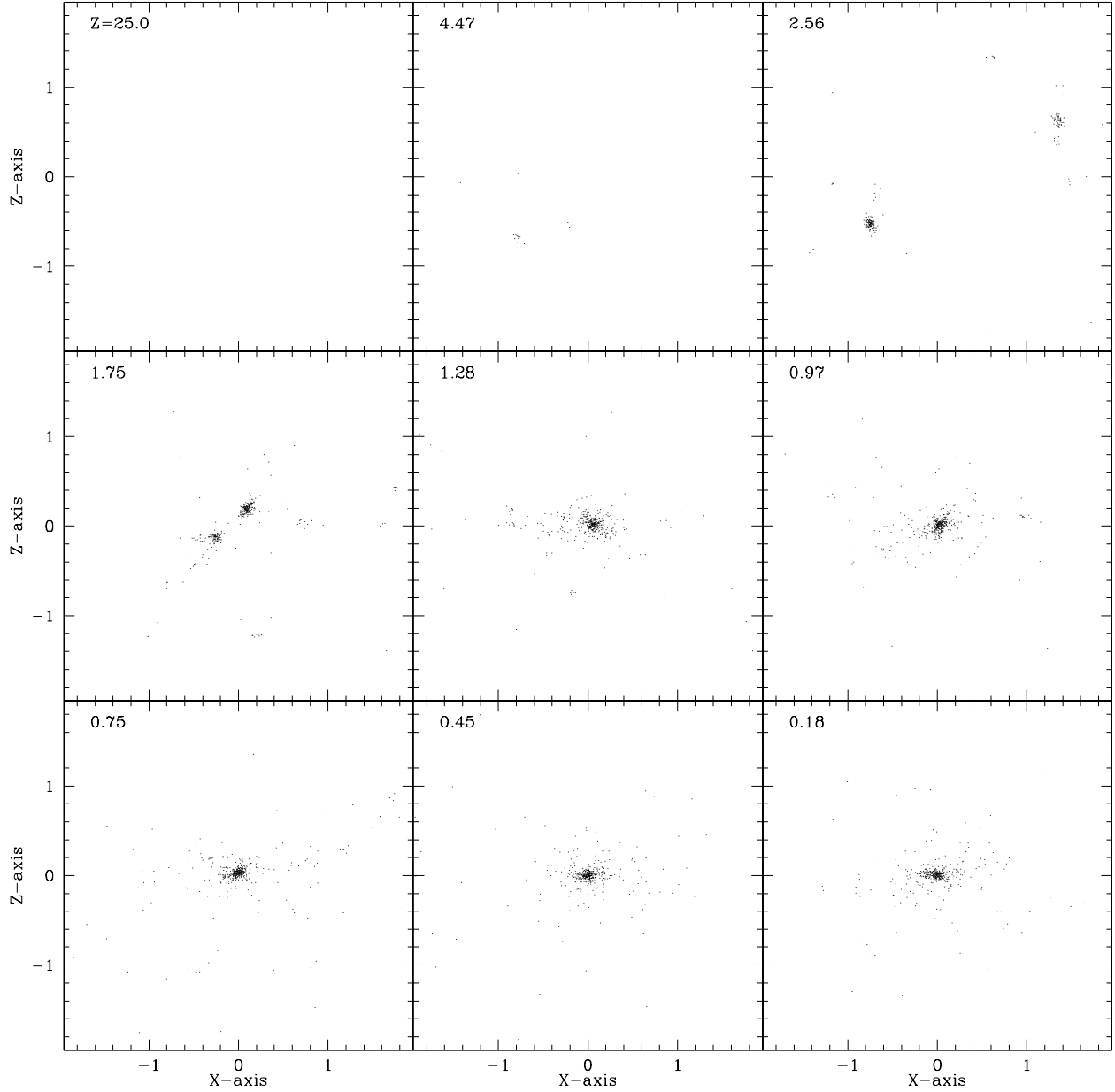


Fig. 9.— Spatial distribution projected onto the x - z plane at each redshift, for stellar particles that finally become metal-poor halo component with metallicity $[\text{Fe}/\text{H}] \leq -1.6$ at $z = 0$. Each frame measures 176 kpc on a side.

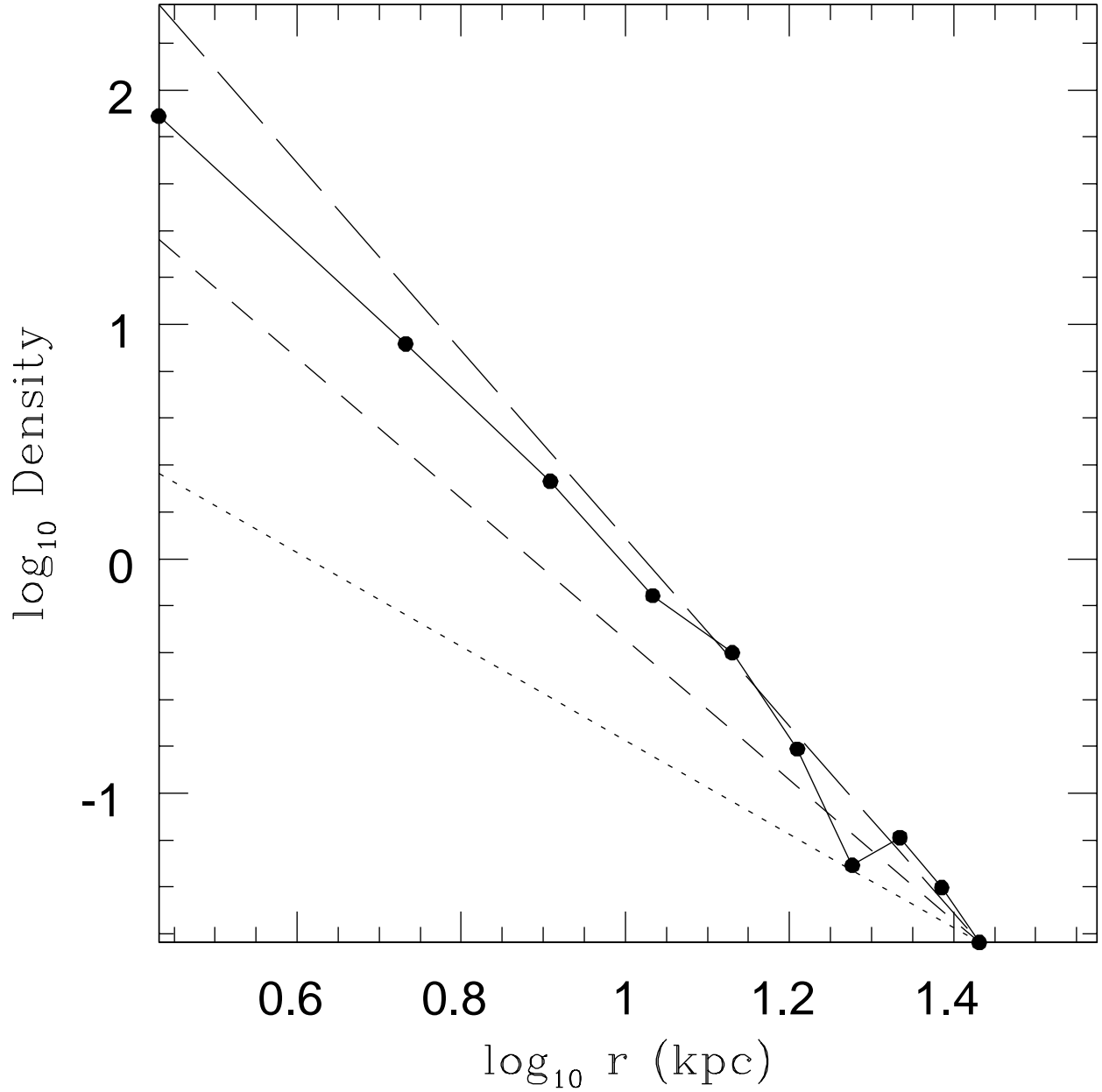


Fig. 10.— Density profile of the simulated stars with $[\text{Fe}/\text{H}] \leq -1.6$ as a function of distance from the center, r (solid line with filled circles). For comparison, the density profiles, $\rho(r) \sim r^{-2}$, r^{-3} , and r^{-4} , are superimposed by dotted, short-dashed, and long-dashed lines, respectively.

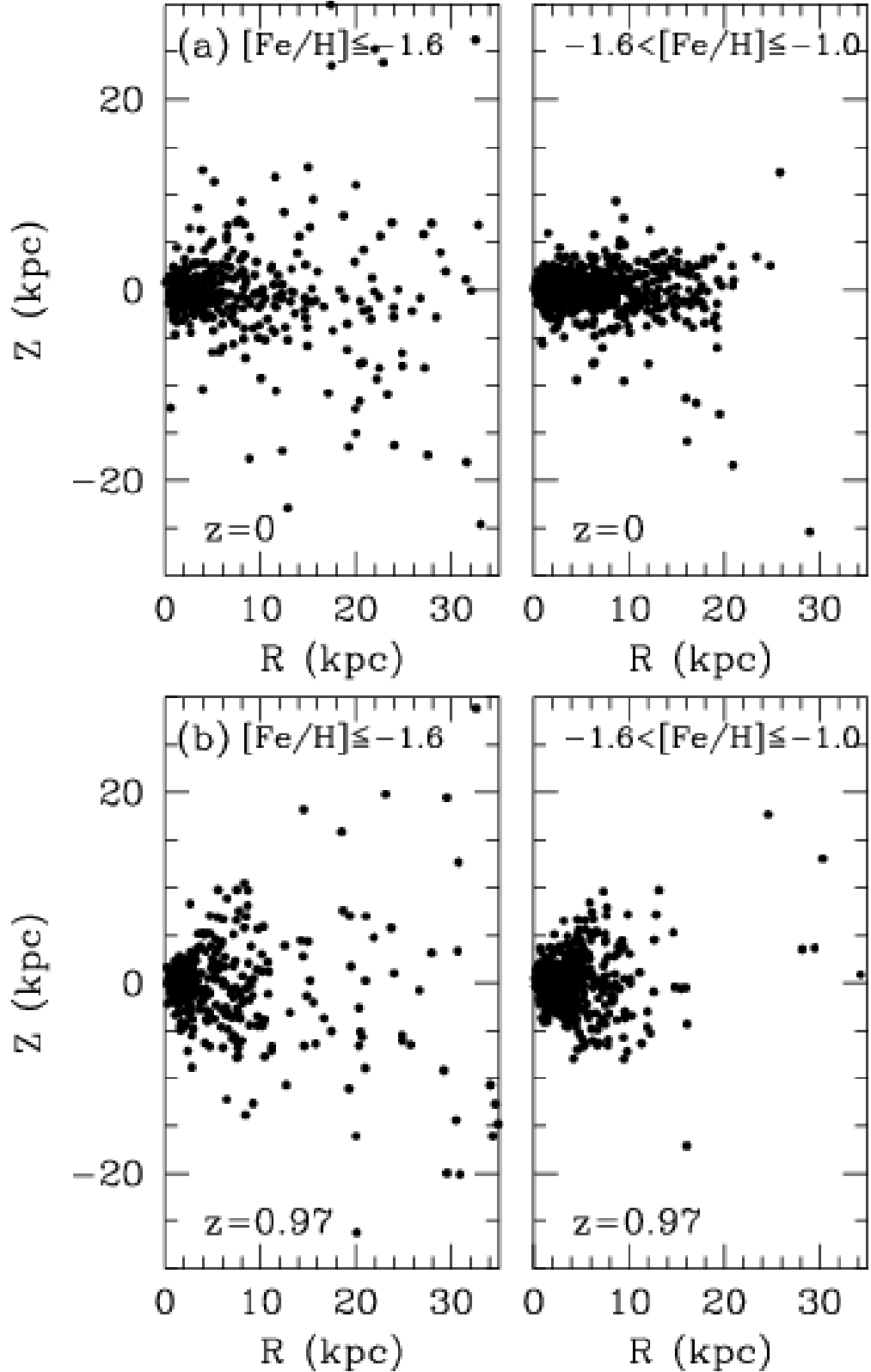


Fig. 11.— Meridional distribution of the stars (within $R = 35$ kpc and $|Z| = 35$ kpc) at $z = 0$ (a) and $z = 0.97$ (b). Left and right panels show the stars with $[\text{Fe}/\text{H}] \leq -1.6$ and $-1.6 < [\text{Fe}/\text{H}] \leq -1$, respectively. The redshift $z = 0.97$ corresponds to the epoch after ~ 1 Gyr passage of the merging event between two massive subgalactic clumps. Note that the hole appears more flattened at $z = 0$ than at $z = 0.97$, as is clearly seen for $-1.6 < [\text{Fe}/\text{H}]$

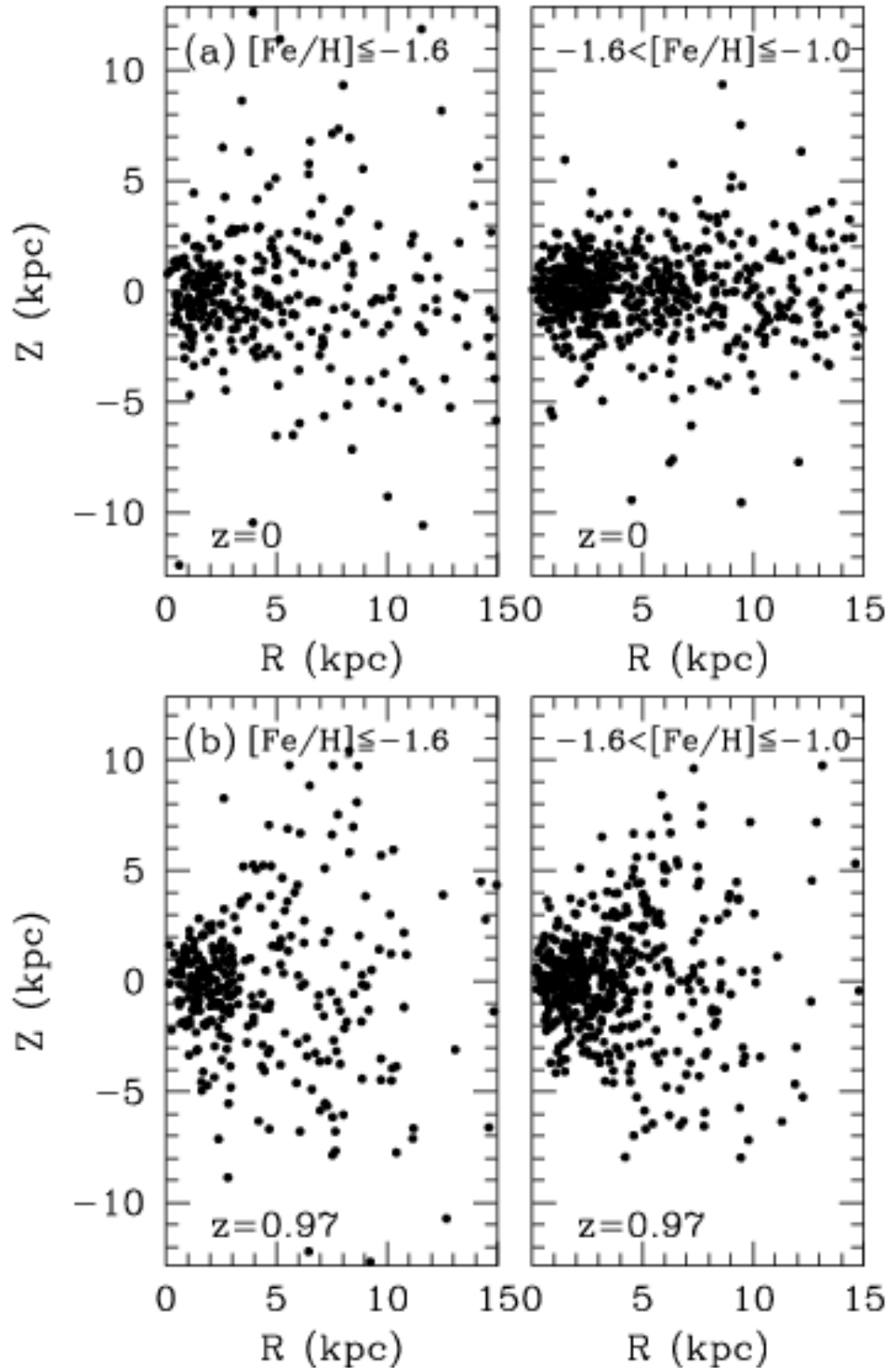


Fig. 12.— The same as Figure 11 but for the stars within $R = 15$ kpc and $|Z| = 15$ kpc.

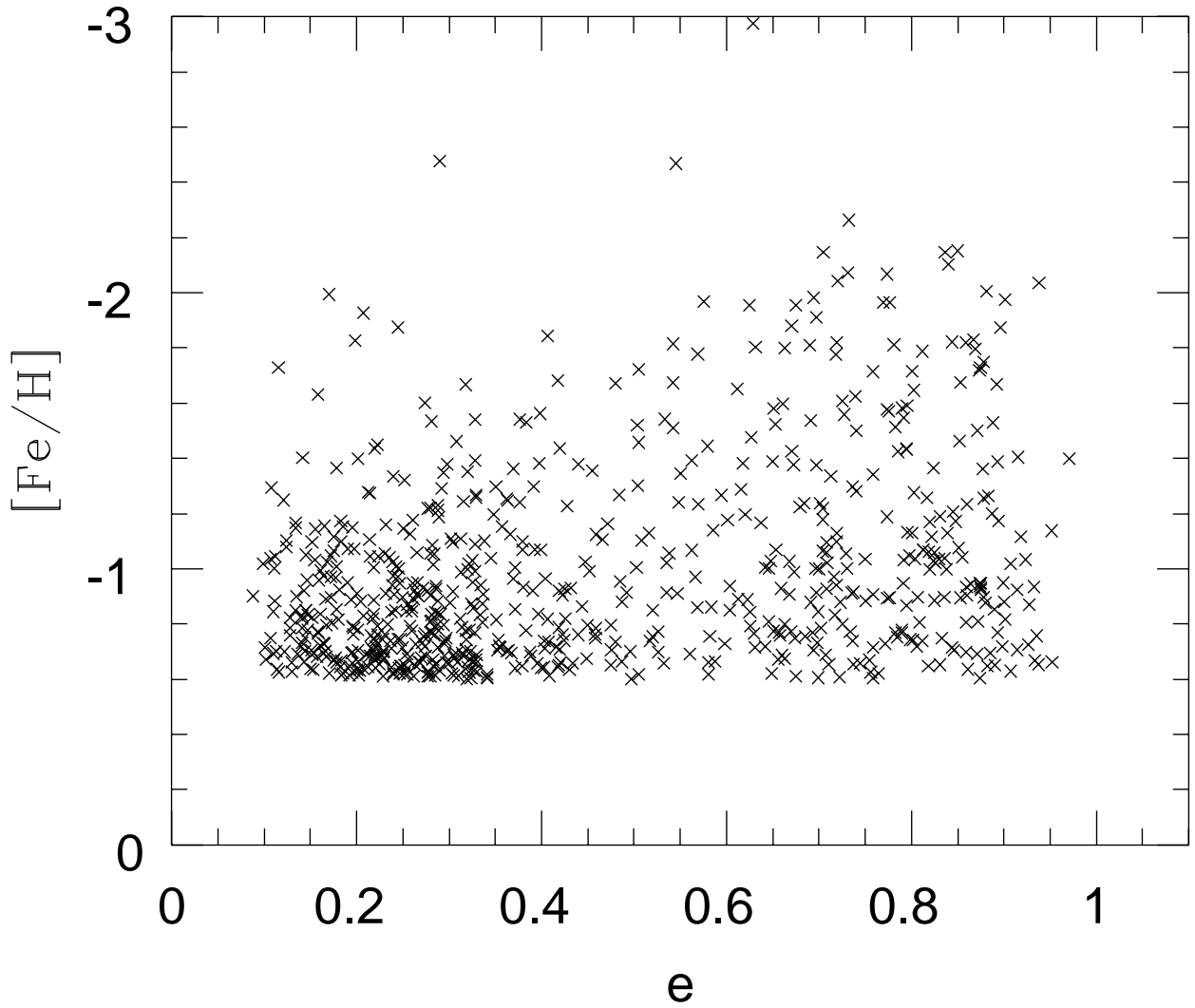


Fig. 13.— Relation between metal abundances ($[Fe/H]$) and orbital eccentricities (e) for the simulated metal-poor stars with $[Fe/H] \leq -0.6$. Note the existence of low- e , low- $[Fe/H]$ stars in the simulated halo.

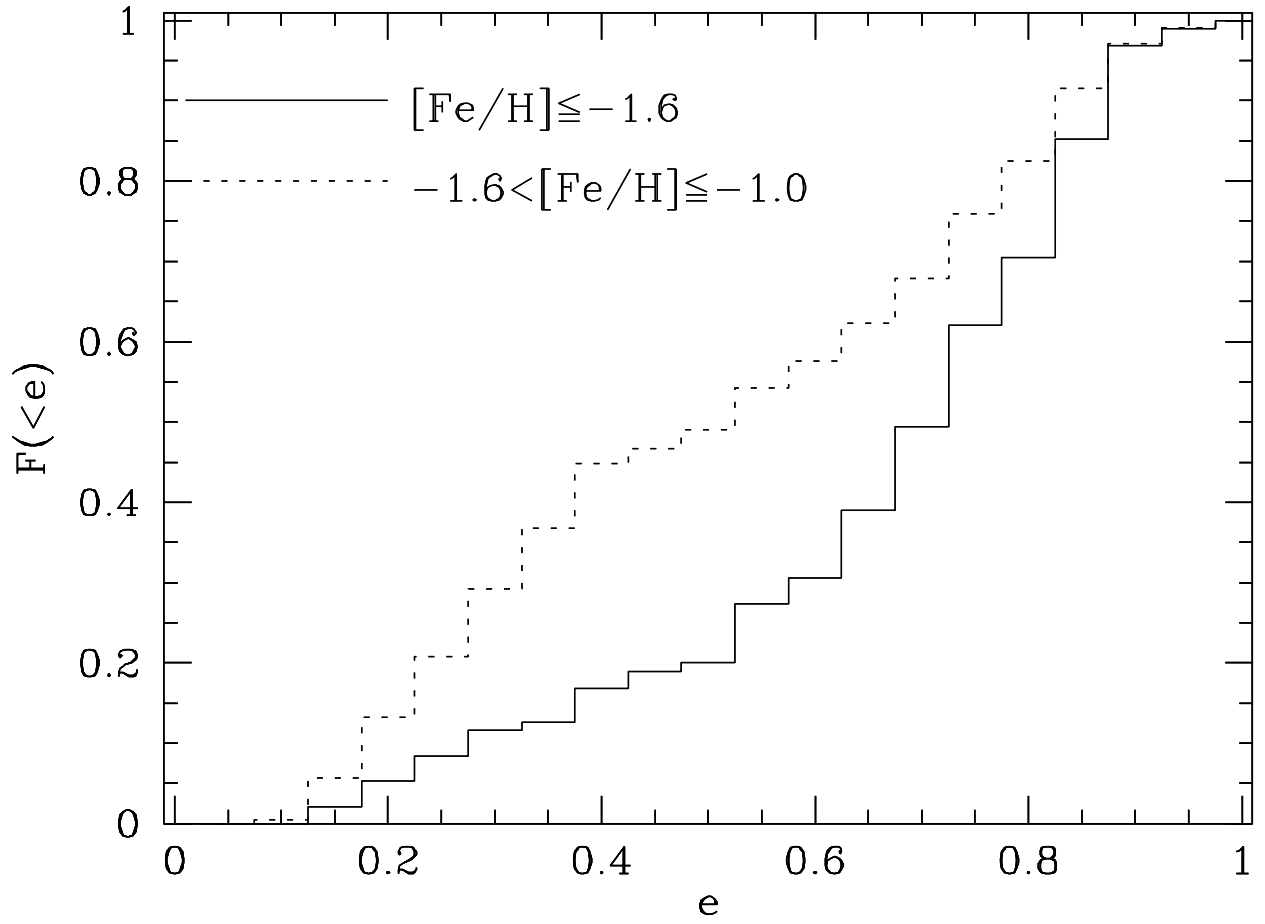


Fig. 14.— Cumulative e distributions, $F(< e)$, in the two abundance ranges of $[\text{Fe}/\text{H}] \leq -1.6$ (solid line) and $-1.6 < [\text{Fe}/\text{H}] \leq -1.0$ (dotted one).

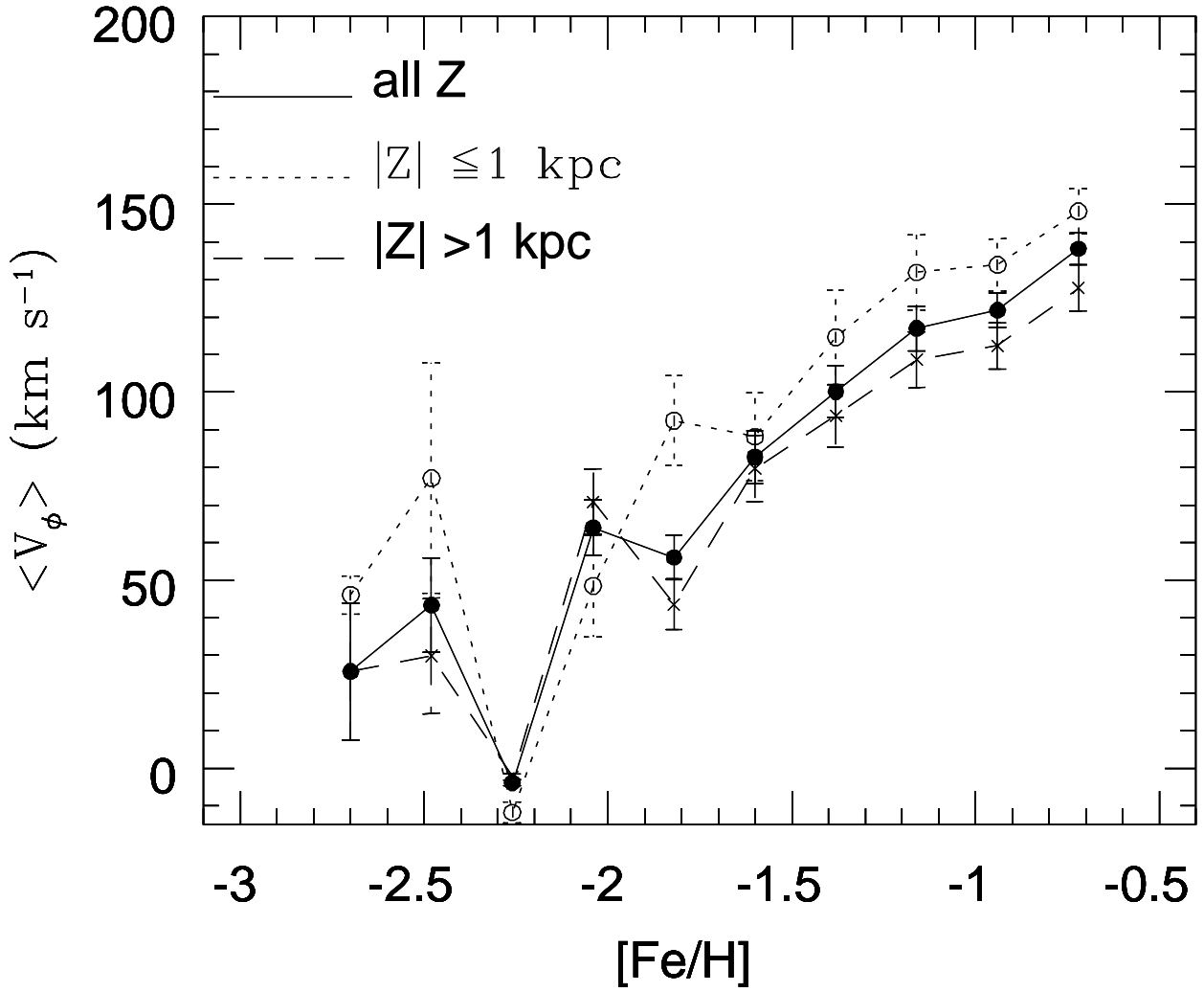


Fig. 15.— Mean rotational velocity $\langle V_\phi \rangle$ vs. metal abundance $[\text{Fe}/\text{H}]$, for all stars (solid line), stars at $|Z| \leq 1$ kpc (dotted line), and at $|Z| > 1$ kpc (dashed line), where Z is the distance from the Galactic plane. Error bars are plotted for each component.

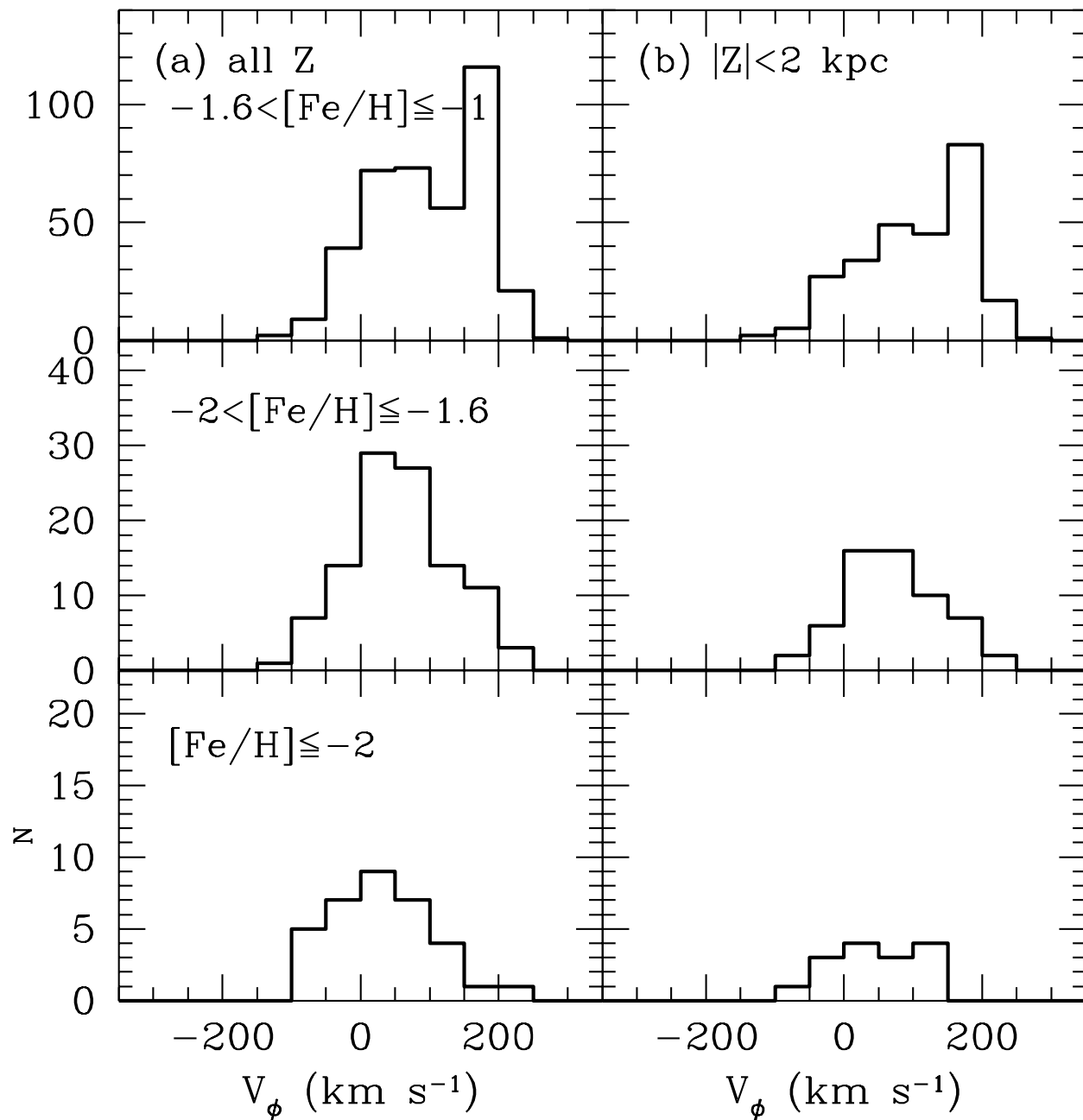


Fig. 16.— Distribution of V_ϕ in different metallicity ranges for the stars at $R > 3$ kpc. Left and right panels denote stars at any $|Z|$ (left panels) and at $|Z| \geq 2$ kpc (right panels), respectively.

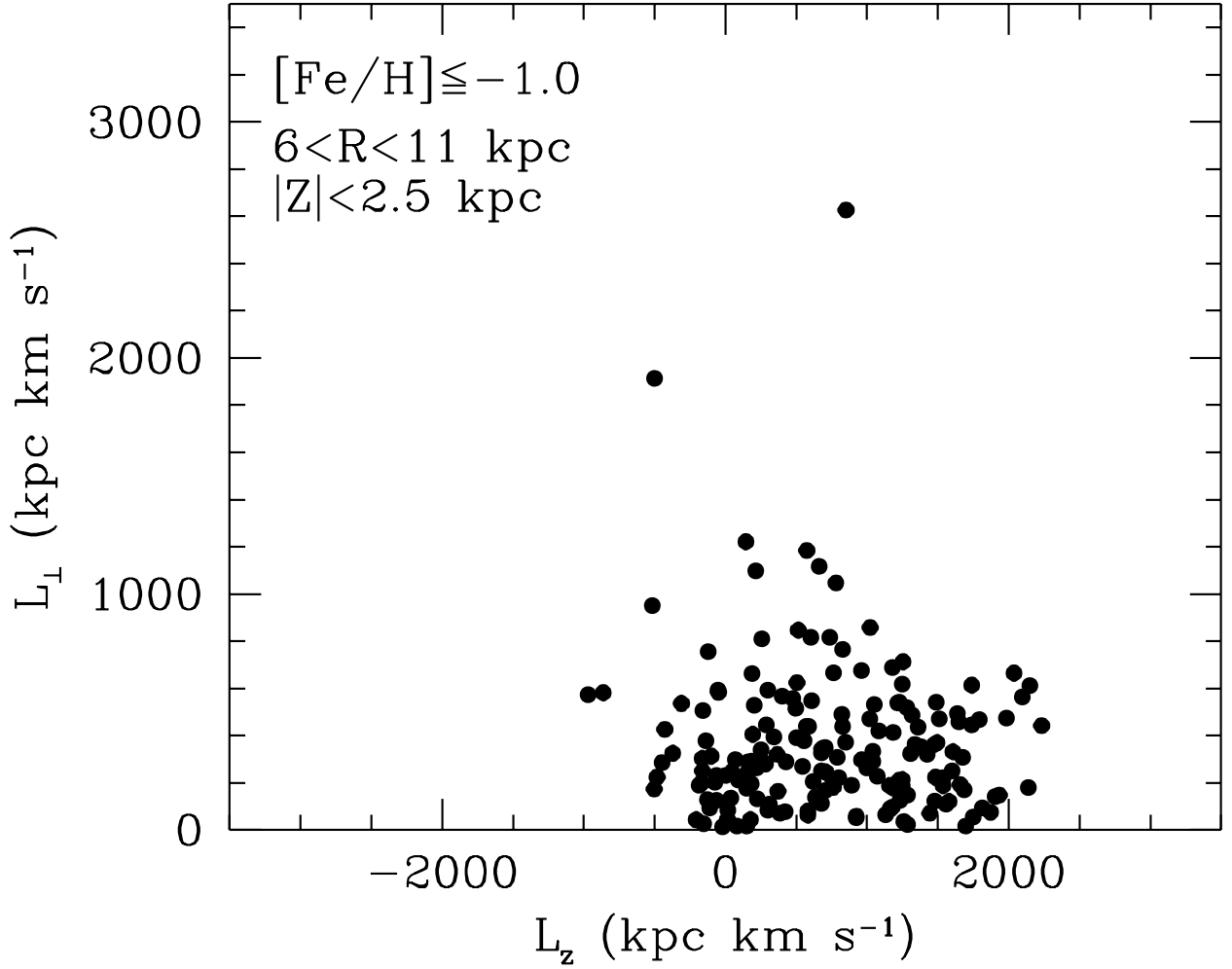


Fig. 17.— The present-day distribution of the simulated stars with $[\text{Fe}/\text{H}] \leq -1.0$ in angular momentum diagram L_z vs. $L_{\perp} = (L_x^2 + L_y^2)^{1/2}$. We have selected the stars at $6 < R < 11$ kpc and $|Z| < 2.5$ kpc, to compare with the observational result near the Sun.

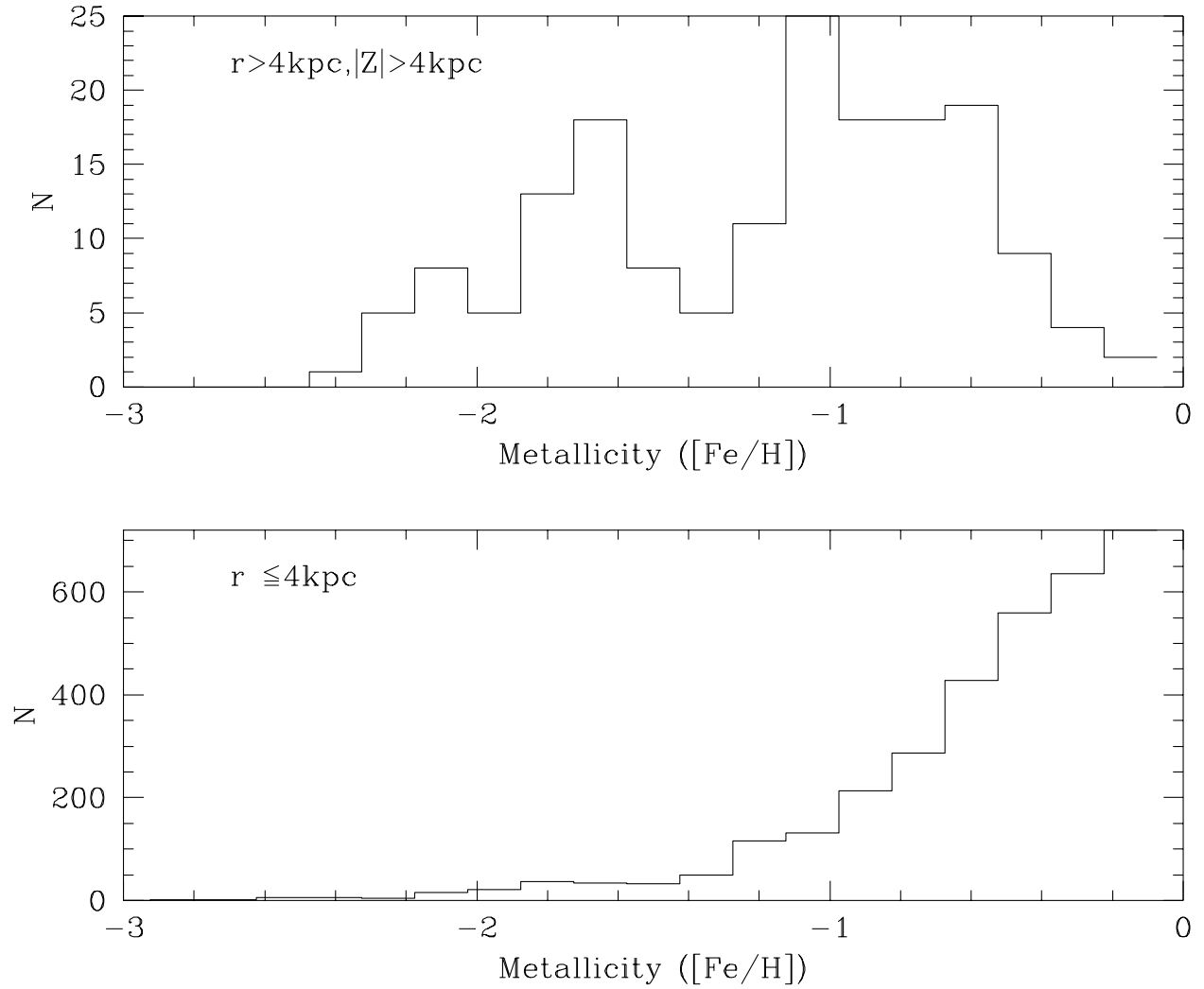


Fig. 18.— Metallicity distributions of the simulated stars at $r > 4$ kpc and $|Z| > 4$ kpc (upper panel) and at $r \leq 4$ kpc (lower panel), respectively. These panels are to be compared with the observed metallicity distributions of the halo and bulge, respectively.

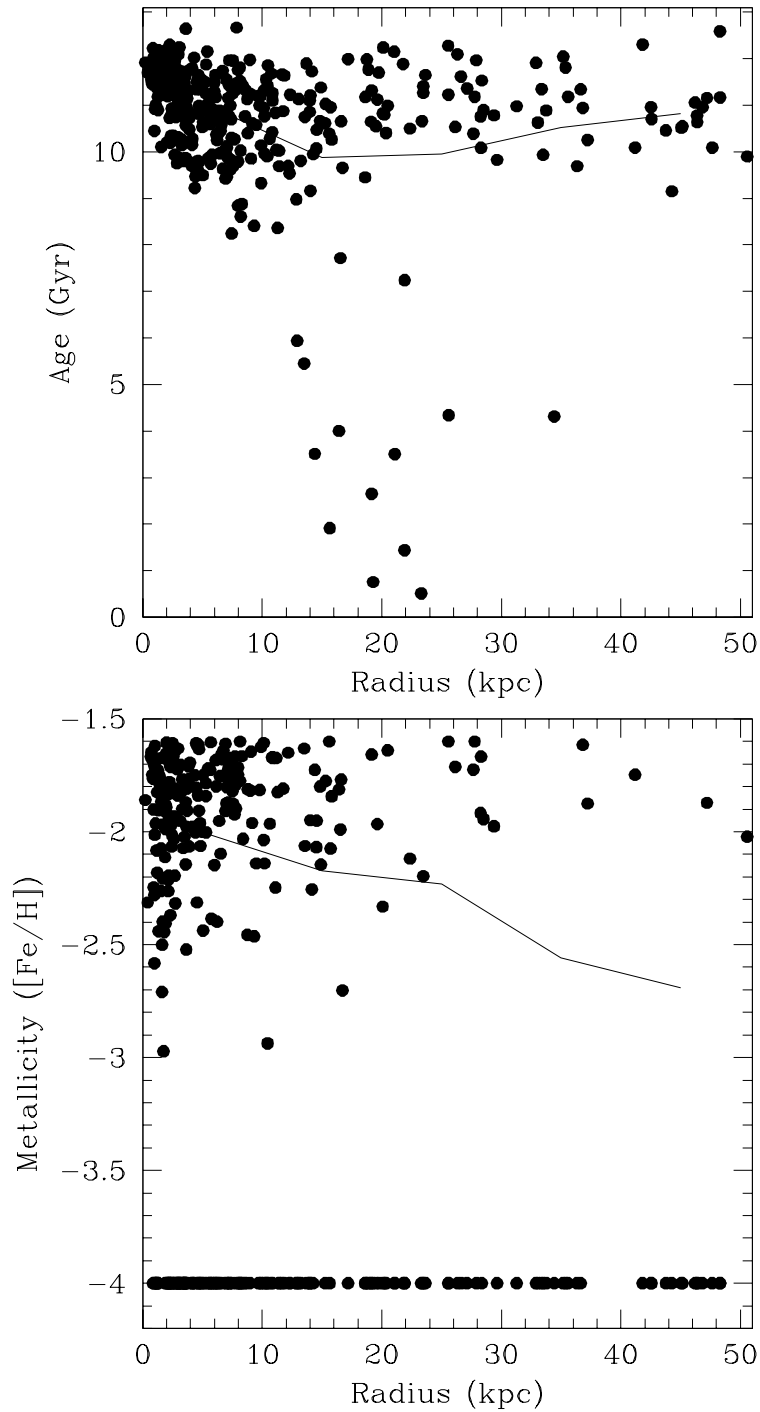


Fig. 19.— Radial distribution of stellar ages (upper panel) and metallicities (lower panel) for the stars with $[\text{Fe}/\text{H}] \leq -1.6$. Solid lines show local regression lines through the points. For convenience, all of the stars with $[\text{Fe}/\text{H}] < -4$ are plotted at $[\text{Fe}/\text{H}] = -4$.

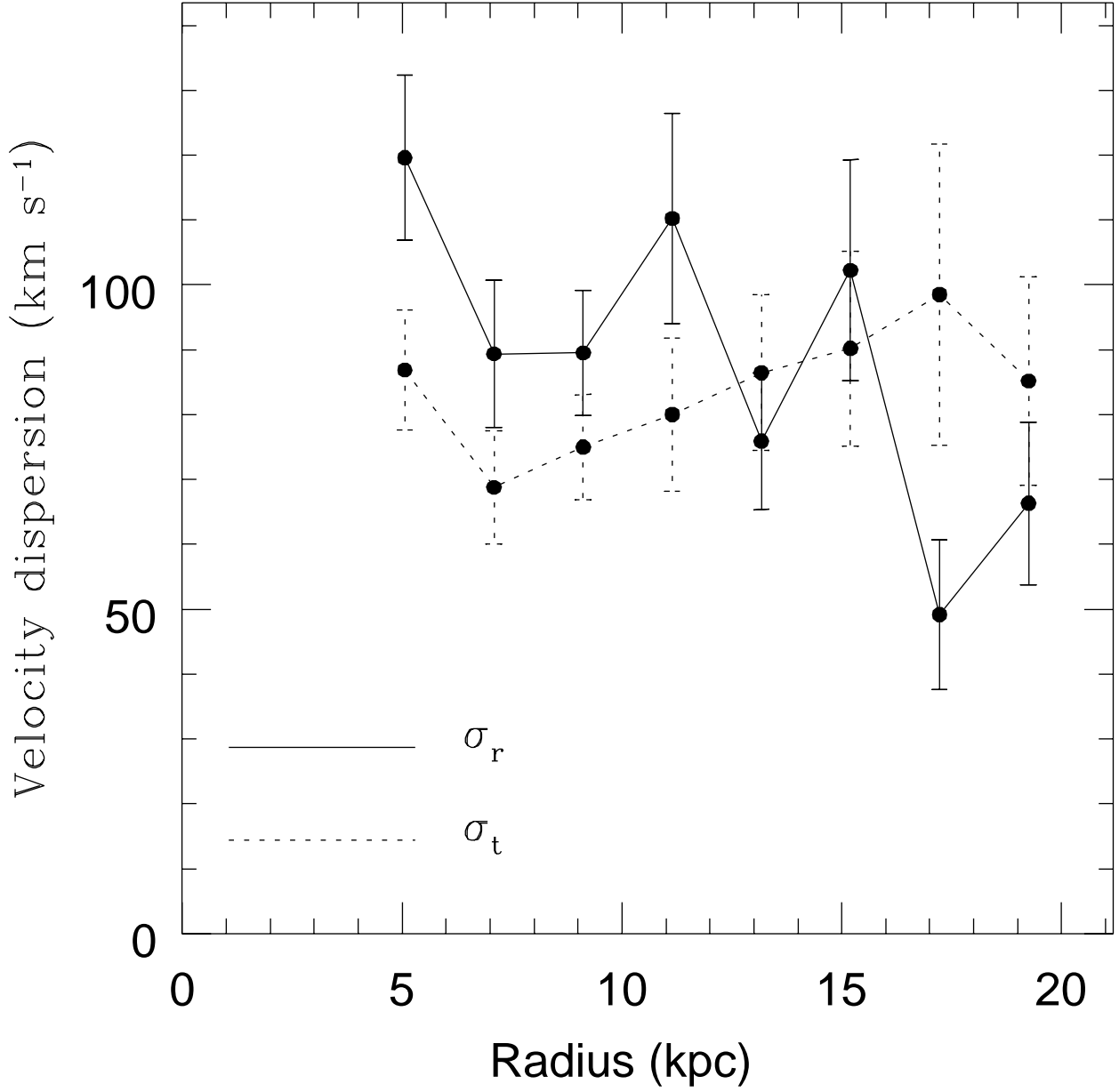


Fig. 20.— Radial dependence of radial velocity dispersion σ_r (solid line) and tangential one σ_t (dotted one) for the stars with $[\text{Fe}/\text{H}] \leq -1.0$ at $|Z| > 2$ kpc. Error bars are plotted for each component.

This figure "f1.gif" is available in "gif" format from:

<http://arxiv.org/ps/astro-ph/0106523v1>

This figure "f2.gif" is available in "gif" format from:

<http://arxiv.org/ps/astro-ph/0106523v1>

This figure "f3.gif" is available in "gif" format from:

<http://arxiv.org/ps/astro-ph/0106523v1>